Nano Research

ISSN 1998-0124 CN 11-5974/O4
https://doi.org/10.26599/NR.2026.94909327

Communication

Engineering built-in electric field in D–A-based covalent organic frameworks for efficient photocatalytic hydrogen evolution

Mingming Xu[1], Pengda Liu[1], Wenhao Huang[1], Shiqi Zhang[1], Jun Xu[2], Zhen Zhou[3], Peng Cheng[1], Wei Shi[1,4](✉)

[1] Frontiers Science Center for New Organic Matter, State Key Laboratory of Advanced Chemical Power Sources and Department of Chemistry, College of Chemistry, Nankai University, Tianjin 300071, China

[2] School of Materials Science and Engineering & National Institute for Advanced Materials, Center for Rare Earth and Inorganic Functional Materials, Tianjin Key Laboratory for Rare Earth Materials and Applications, Nankai University, Tianjin 300350, China

[3] School of Materials Science and Engineering, Institute of New Energy Material Chemistry, Nankai University, Tianjin 300350, China

[4] State Key Laboratory of Elemento-Organic Chemistry, Nankai University, Tianjin 300071, China

Nano Res., **Just Accepted Manuscript** • https://doi.org/10.26599/NR.2026.94909327

https://www.sciopen.com/journal/1998-0124 on Nov. 12, 2026

© The Authors(s)

Just Accepted

This is a “Just Accepted” manuscript, which has been examined by the peer-review process and has been accepted for publication. A “Just Accepted” manuscript is published online shortly after its acceptance,which is prior to technical editing and formatting and author proofing. Tsinghua University Press (TUP) provides “Just Accepted” as an optional and free service which allows authors to make their results available to the research community as soon as possible after acceptance. After a manuscript has been technically edited and formatted, and the page proofs have been corrected, it will be removed from the “Just Accepted” web site and published officially with volume and article number (e.g., *Nano Research*, **2025**, *18*, 94906990). Please note that technical editing may introduce minor changes to the manuscript text and/or graphics which may affect the content, and all legal disclaimers that apply to the journal pertain. In no event shall TUP be held responsible for errors or consequences arising from the use of any information contained in these “Just Accepted” manuscripts. To cite this anuscript please use its Digital Object Identifier (DOI®),which is identical for all formats of publication.

Communication

Engineering built-in electric field in D–A-based covalent organic frameworks for efficient photocatalytic hydrogen evolution

Mingming Xu [1], Pengda Liu [1], Wenhao Huang [1], Shiqi Zhang [1], Jun Xu [2], Zhen Zhou [3], Peng Cheng [1], Wei Shi [1,4]

[1] Frontiers Science Center for New Organic Matter, State Key Laboratory of Advanced Chemical Power Sources and Department of Chemistry, College of Chemistry, Nankai University, Tianjin 300071, China
[2] School of Materials Science and Engineering & National Institute for Advanced Materials, Center for Rare Earth and Inorganic Functional Materials, Tianjin Key Laboratory for Rare Earth Materials and Applications, Nankai University, Tianjin 300350, China
[3] School of Materials Science and Engineering, Institute of New Energy Material Chemistry, Nankai University, Tianjin 300350, China
[4] State Key Laboratory of Elemento-Organic Chemistry, Nankai University, Tianjin 300071, China

Received: 11 September 2026; **Revised: 3 November 2026**; **Accepted: 12 November 2026**

Address correspondence to Wei Shi, shiwei@nankai.edu.cn

Cite this article: *Nano Research*, 2027, 20, 94909327 https://doi.org/10.26599/NR.2026.94909327

ABSTRACT: The built-in electric field (BIEF) of photocatalysts plays an important role in the separation and transport efficiency of photogenerated charge carriers and hence governs the photocatalytic activity. Herein, we report the one-pot gram-scale synthesis of three isostructural donor–acceptor (D–A) based covalent organic frameworks with regulated BIEF using ethanol as a green solvent. Through engineering the asymmetric electronic configuration of the donor component without changing the main framework, promoted photocatalytic hydrogen evolution rate from 2.3 to 31.8 mmol g^{-1} h^{-1} was achieved. Comprehensive mechanism studies reveal that the BIEF strength was significantly enhanced by the fine regulation of donor component, enabling efficient photogenerated charge carrier transport, and suppressing their recombination, thereby inducing a high hydrogen evolution rate. This work not only provides an efficient way for the green synthesis of D–A-based covalent organic frameworks, but also gains insight into the influence of BIEF based on uniformly arranged D–A components for the development of advanced photocatalysts.

KEYWORDS: built-in electric field; donor–acceptor covalent organic frameworks; green synthesis; gram-scale synthesis; photocatalytic hydrogen evolution.

1. Introduction

The development of clean and environmentally friendly energy sources is of vital importance for alleviating the global energy and ecological crises [1–4]. As a clean and sustainable energy, hydrogen plays a pivotal role owing to its high energy density and carbon-neutral nature [5–8]. Nevertheless, conventional hydrogen production methods are still energy-intensive and emit substantial amounts of CO_2 [9,10]. Harnessing solar energy for photocatalytic water splitting to generate hydrogen has thus emerged as a promising strategy [11–13]. To develop efficient photocatalysts, factors including spectral absorption and band structures have been systematically studied [14–16]. Besides these energy-related factors, the built-in electric field (BIEF) provides the driving force for charge separation and facilitates the migration of charge carriers to the surface of photocatalyst, which governs the efficiency of photocatalytic activity [17–20]. However, modulating the chemical components of photocatalysts to enhance the BIEF remains highly challenging, primarily due to the unclear structure-function relationship in such complex systems.

Covalent Organic Frameworks (COFs) are a class of porous materials constructed through the covalent linkage of organic building blocks [21–30]. With broad-spectrum light absorption and tunable band structures, COFs have emerged as a versatile platform for integrating multiple photocatalytic units into a single material [31–41]. However, owing to their low dielectric constants, conventional COFs generally exhibit relatively high exciton binding energies, which are detrimental to photocatalytic activity [42–46]. Introducing ordered D–A components into COFs renders the charge distribution within the framework asymmetric, generating BIEF that provides a driving force for charge separation and lowers the exciton binding energies, thus suppressing charge-carrier recombination [47–57]. Due to the high complexity in regulating D and A molecules in terms of energy level alignment, spatial configuration, and intermolecular interactions, achieving the alternating and ordered arrangement of D–A units within COF framework to create a strong BIEF remains a significant challenge.

Herein, three D–A COFs, NKU-331, NKU-332, and NKU-333 were synthesized at the gram scale via a one-pot reaction using ethanol as solvent, where biaryls (biphenyl, phenyl-pyridine and bipyridine) served as the electron donor and guanidinium acted as the electron acceptor.

Just Accepted

Guanidinium is characterized by a highly delocalized positive charge and strong electron-withdrawing ability, making it a

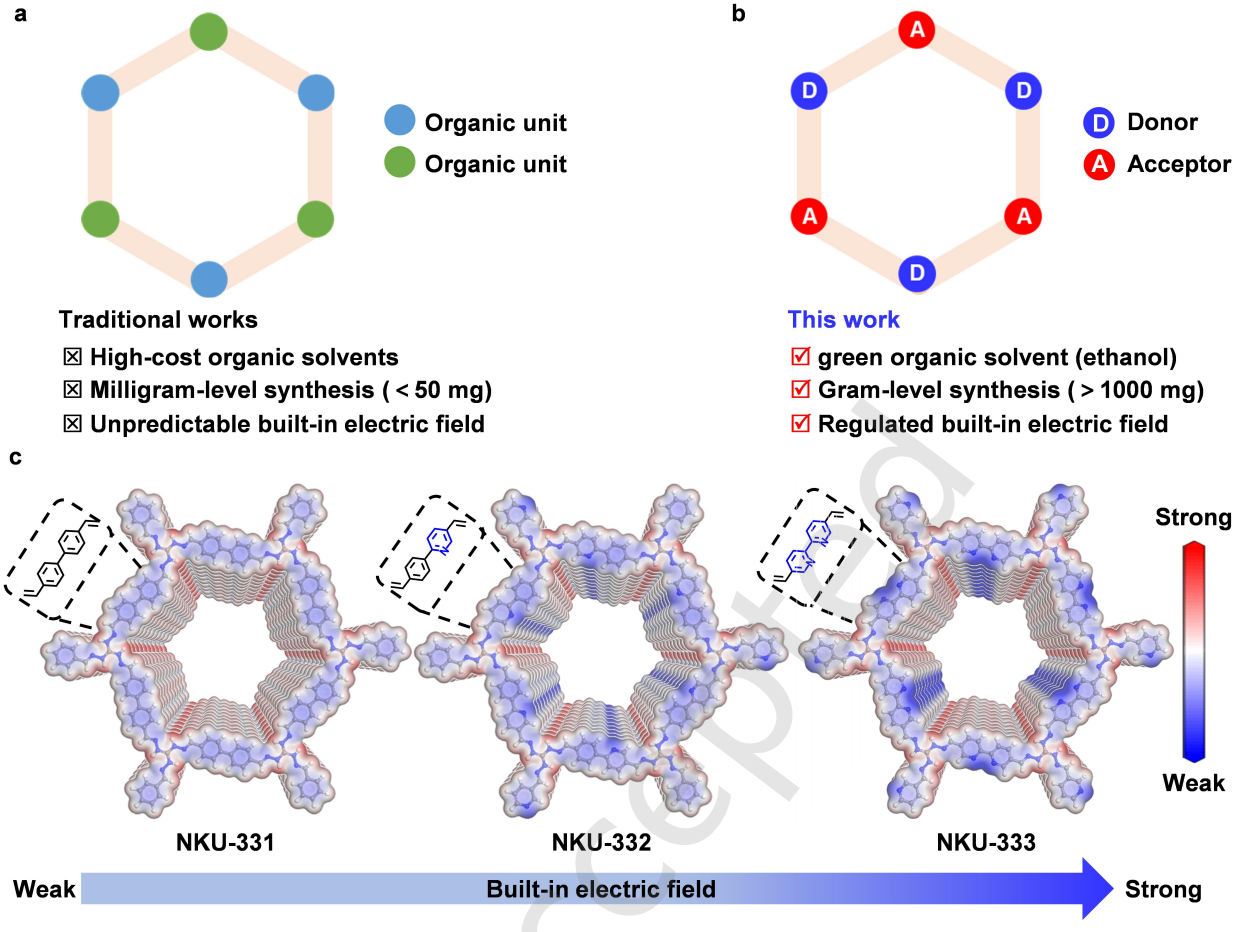

Figure 1. (a,b) Comparison of synthetic strategies of COFs. (c) Structures and electrostatic potential distribution of NKU-331–333.

promising acceptor [58]. By regulating the donor units without altering the overall structure of the COFs, we achieved a significant enhancement in the photocatalytic hydrogen production rate from 2.3 mmol g^{-1} h^{-1} of NKU-331 to 31.8 mmol g^{-1} h^{-1} of NKU-333 (Fig. 1). A systematic mechanistic study revealed that precise regulation of the donor group significantly enhanced the BIEF to promote the separation and transport of photogenerated charge carriers, effectively suppress their recombination, and ultimately lead to the outstanding hydrogen evolution activity. This work not only provides a facile strategy for the green and large-scale synthesis of D–A COFs but also gains insight into the role of BIEF formed by ordered D–A units for the development of high-performance photocatalysts.

2. Experimental

2.1 Synthesis of NKU-331

NKU-331 was synthesized by the Schiff-base reaction between tris(amino)guanidinium chloride (422 mg, 3.0 mmol) and 4,4'-biphenyldicarboxaldehyde (946 mg, 4.5 mmol) in 60 mL anhydrous ethanol with 3.0 mL 6.0 M acetic acid as solvent. The reaction mixture was transferred into a 100 mL autoclave, purged with nitrogen for 0.5 h, and then heated at 120 °C for 72 h. After cooling to room temperature, the product was washed with ethanol. The product was dried at 85 °C for 12 h to obtain a yellow solid. Yield: 95% (based on 4,4'-biphenyldicarboxaldehyde).

2.2 Synthesis of NKU-332

Except for the use of 4-(5-formylpyridin-2-yl)benzaldehyde (951 mg, 4.5 mmol) instead of 4,4'-biphenyldicarboxaldehyde, the other processes are the same as for NKU-331. NKU-332 was dried at 85 °C for 12 h to obtain an orange solid. Yield: 95% (based on 4-(5-formylpyridin-2-yl)benzaldehyde).

2.3 Synthesis of NKU-333

Except for the use of 2,2'-bipyridyl-5,5'-dialdehyde (955 mg, 4.5 mmol) instead of 4,4'-biphenyldicarboxaldehyde, the others are the same as for NKU-331. NKU-333 was dried at 85 °C for 12 h to obtain an orange solid. Yield: 96% (based on 2,2'-Bipyridyl-5,5'-dialdehyde).

3. Results and discussion

NKU-331–333 were synthesized via Schiff-base reactions between triaminoguanidine hydrochloride and biaryls (biphenyl, phenyl-pyridine, and bipyridine) aldehydes in ethanol (Fig. 1). Powder X-ray diffraction (PXRD) patterns of them all displayed distinct peaks at 3.85°, assigned to the (100) facet of a primitive lattice (Figs. 2(a)–2(c)) [59]. The simulations of the PXRD patterns indicate that they all adopt an overlapping AA-type arrangement and crystallize isostructurally in the triclinic *P*1 space group [60, 61]. Herein, the structure of NKU-333 is representatively described. The triaminoguanidine acts as a 3-connected node, covalently bonded to three bipyridine via imine bonds

Just Accepted

formed through Schiff-base condensation. The triaminoguanidine and bipyridine units are arranged in a periodic and homogeneous manner, with chloride counterions associated with the protonated triaminoguanidine nodes to maintain charge neutrality, which further extends to form a two

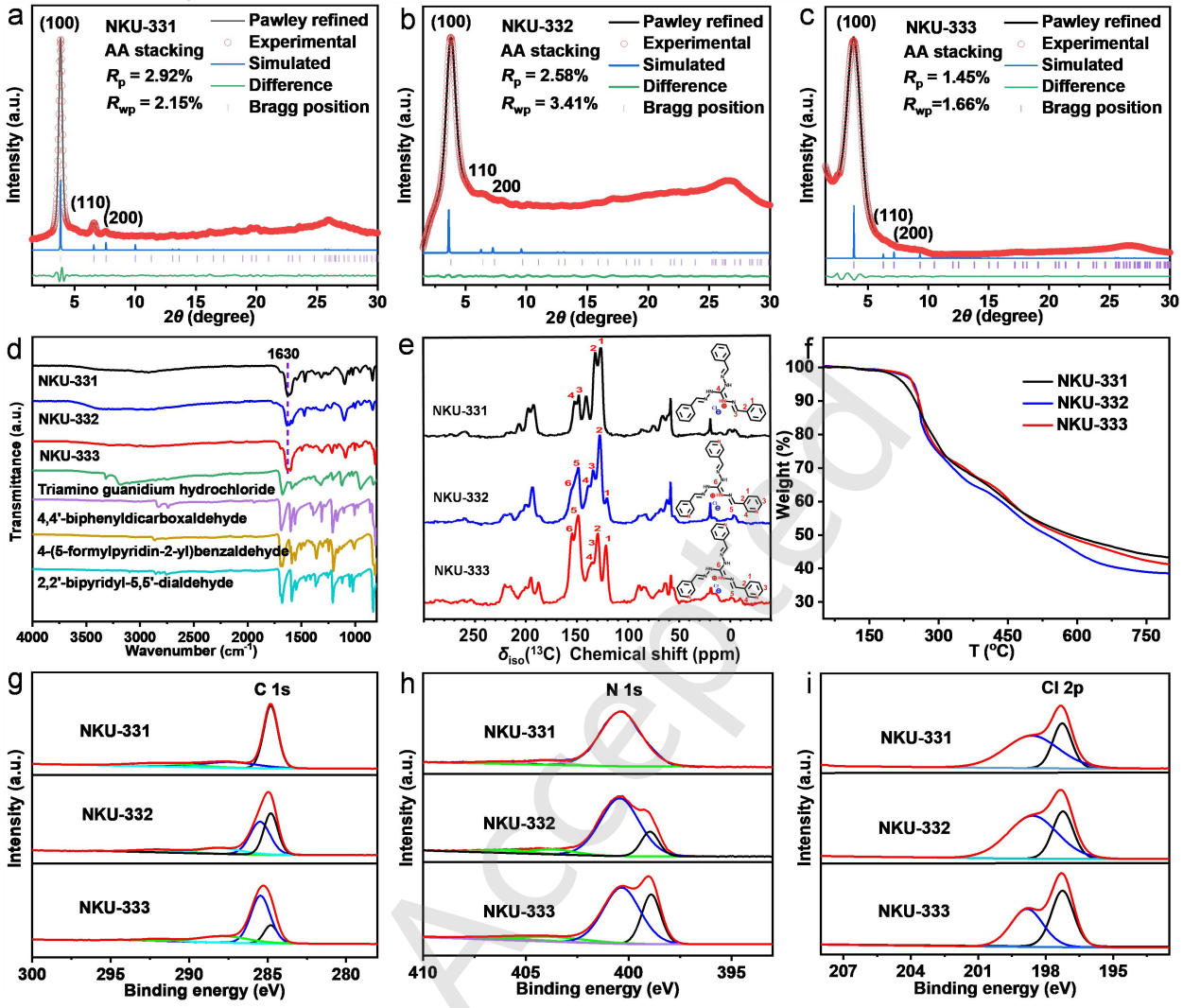

Figure 2. PXRD patterns of NKU-331 (a), NKU-332 (b), and NKU-333 (c). (d) FTIR spectra, (e) Solid-state 13C CP-MAS NMR spectra and (f) thermogravimetric analysis of NKU-331–333. (g) C 1s, (h) N 1s, and (i) Cl 2p XPS spectra of NKU-331–333.

dimensional honeycomb-like network (Figure 1), with the unit cell parameters of a = 3.5286 Å, b = 28.1515 Å, c = 28.1785 Å, α = 119.9°, β = 90°, γ = 90°.

The Fourier transform infrared (FTIR) spectra showed characteristic absorption peaks at 1630 cm^{-1} for all three COFs, indicating the formation of imine bonds (Fig. (2d)) [62, 63]. Solid-state ^{13}C cross-polarization magic angle spinning (CP-MAS) nuclear magnetic resonance (NMR) spectra were further measured (Fig. (2e)). The peak at 148 ppm corresponding to the imine carbon, confirming the formation of imine bonds as well [64–67]. Thermogravimetric analysis (Fig. (2f)) and variable temperature PXRD patterns (Figs. (S1)–(S3)) demonstrate that these COFs have good thermal stabilities up to 400 K. Furthermore, NKU-331–333 are stable in common solvents (Figs. (S4)–(S6)).

X-ray photoelectron spectroscopy (XPS) measurements of NKU-331–333 were performed. In the C 1s spectra (Fig. (2g)), all COFs exhibit characteristic peaks at 284.8 eV, corresponding to C=C/C–C bonds and confirming the presence of the benzene ring in aromatic backbone. Another peak was found at 285.6 eV for NKU-332 and NKU-333, which is assigned to C–N of the pyridine ring [68, 69]. In the N 1s spectra (Fig. (2h)), all COFs have characteristic peaks at 400.4 eV, corresponding to the C=N bonds from the formation of imine linkages. Besides this peak, additional peaks of pyridine N appeared at 398.9 eV for NKU-332 and NKU-333 [70]. The Cl 2p spectra were deconvoluted into two components at 197.3 and 198.6 eV (Fig. (2i)), corresponding to Cl $2p_{3/2}$ and Cl $2p_{1/2}$ orbitals, respectively [71].

The morphologies of NKU-331–333 were characterized by scanning electron microscopy (SEM) (Figs. (S7–S9)). NKU-331 and NKU-332 are irregular nanofibrous, and NKU-333 is nanosheets. Static water contact angle measurements showed that NKU-331–333 had contact angles of 56.5°, 52.7°, and 50.9°, respectively, indicating they are hydrophilic (Fig. (S10)). The N_2 adsorption isotherms showed that NKU-331–333 have limited N_2 uptake capacity and low porosity (Figs. (S11)–(S13)), due to the presence of chloride anions in the channels [64, 72].

The light capturing abilities of NKU-331–333 were evaluated by UV-vis spectra, revealing that they all have strong light capturing capacity (Fig. (3a)). The band gaps of

Just Accepted

NKU-331, NKU-332 and NKU-333 calculated by Tauc plots are 2.30, 2.06 and 2.02 eV, respectively (Fig. (3b)). In addition, the photocatalytic activity of photocatalysts also depends on their conduction band (CB) and valence band (VB). Mott-Schottky curves were plotted to identify the flat band

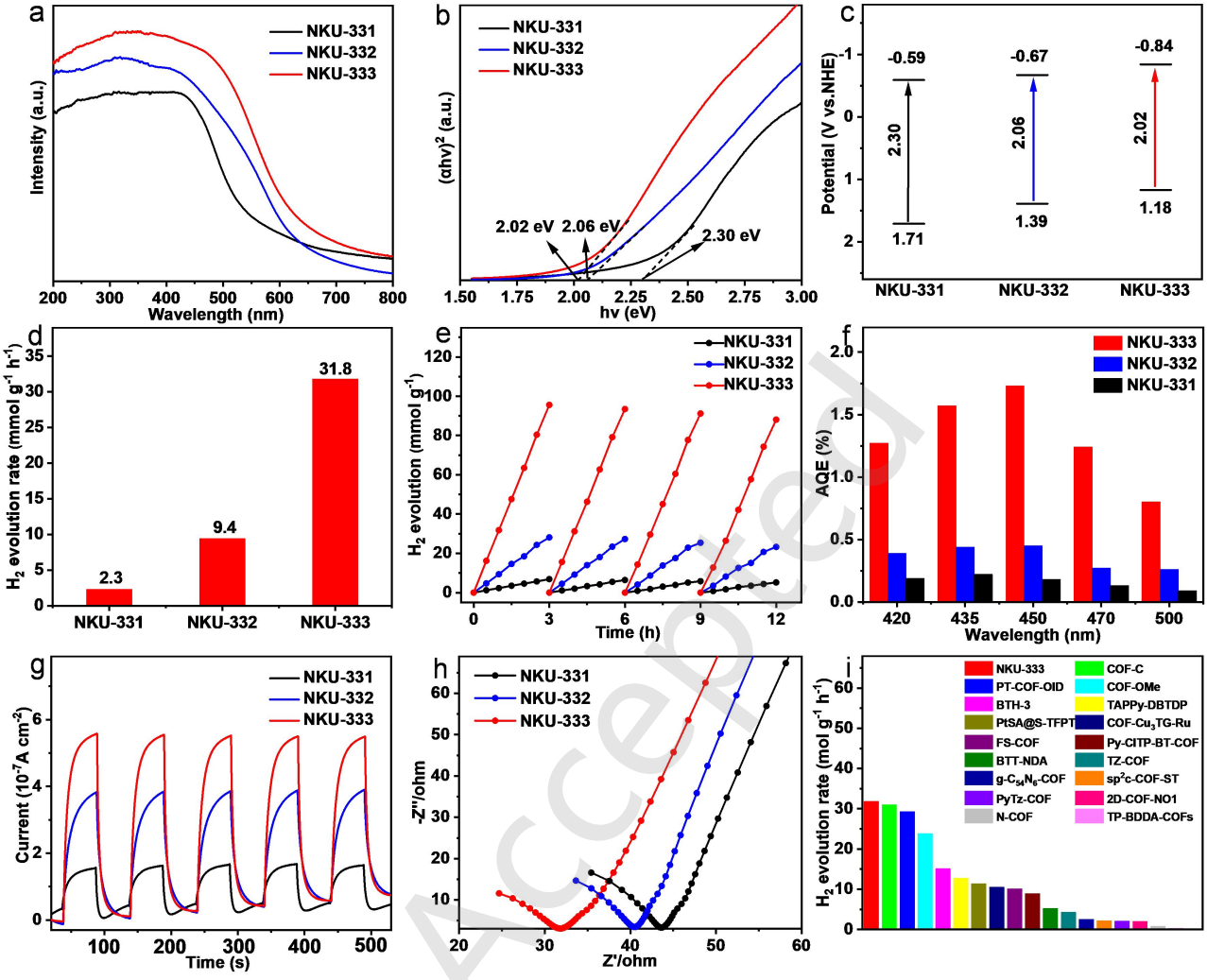

Figure 3. (a) UV-Vis diffuse-reflectance spectra, (b) Tauc plots, (c) Band structures, (d) Photocatalytic hydrogen evolution rates, (e) Multiple cycles of photocatalytic hydrogen evolution, (f) AQE comparison, (g) Transient photocurrent responses and (h) Nyquist plots of NKU-331–333. (i) The comparison of hydrogen production activities with selected COF-based photocatalysts.

positions (Figs. (S14)–(S16)). The slopes of NKU-331–333 were all positive, indicating n-type semiconductors. As the CB potential of n-type semiconductor is generally ~0.2 V more negative than the flat band, the CB potentials were −0.59, −0.67, and −0.84 V versus NHE for NKU-331, NKU-332 and NKU-333, respectively. According to the CB potentials and band gaps, the VB positions of them were 1.71, 1.39, and 1.18 V versus NHE, respectively (Fig. (3c)). The optical band gap narrows from 2.30 to 2.02 eV, and the conduction band edge shifts to a more negative potential on going from NKU-331 to NKU-333, which are thermodynamically favorable for HER.

NKU-331–333 exhibited exceptional hydrophilicity, high stability, and suitable band structures, highlighting their potential as photocatalysts for hydrogen evolution via water splitting. The photocatalytic hydrogen evolution performances of NKU-331–333 were evaluated by dispersing them in aqueous solution containing ascorbic acid as a sacrificial agent and H_2PtCl_6 as a co-catalyst under visible light (>420 nm). NKU-331, NKU-332 and NKU-333 exhibited photocatalytic hydrogen evolution activities of 2.3, 9.4, and 31.8 mmol g^{-1} h^{-1}, respectively, and NKU-333 achieved the highest hydrogen evolution rate, which is 13.8 times higher than that of NKU-331 (Fig. (3d)). NKU-331–333 maintained stable hydrogen evolution rates during 12 h cycling tests under visible light (Fig. (3e)). The PXRD patterns showed no noticeable changes before and after the reaction, demonstrating the high stability and activity of NKU-331–333 (Figs. (S17)–(S19)). The wavelength-dependent apparent quantum yield (AQE) of NKU-333 reaches 1.73% at 450 nm (Fig. (3f)), demonstrating its high efficiency in converting visible light into photogenerated electrons for proton reduction.

Photoelectrochemical measurements were performed to investigate the behavior of photoexcited charge carriers. The photocurrent response of NKU-333 was significantly stronger than those of NKU-331 and NKU-332, confirming its more efficient charge separation and transport (Fig. (3g)). In the electrochemical impedance spectroscopy (EIS) measurements, the Nyquist arc radii decrease from NKU-331 to NKU-333, which matched the trend of their photocatalytic hydrogen evolution activities (Fig. (3h)). NKU-333 exhibits

Just Accepted

higher photocatalytic hydrogen evolution activity than previously reported COF-based photocatalysts, representing one of the most promising HER photocatalysts reported to date (Fig. (3i) and Table S1).

In the photoluminescence (PL) spectra (Fig. (4a)), the emission intensity of NKU-333 was the weakest compared with NKU-331 and NKU-332, indicating that NKU-333 has a

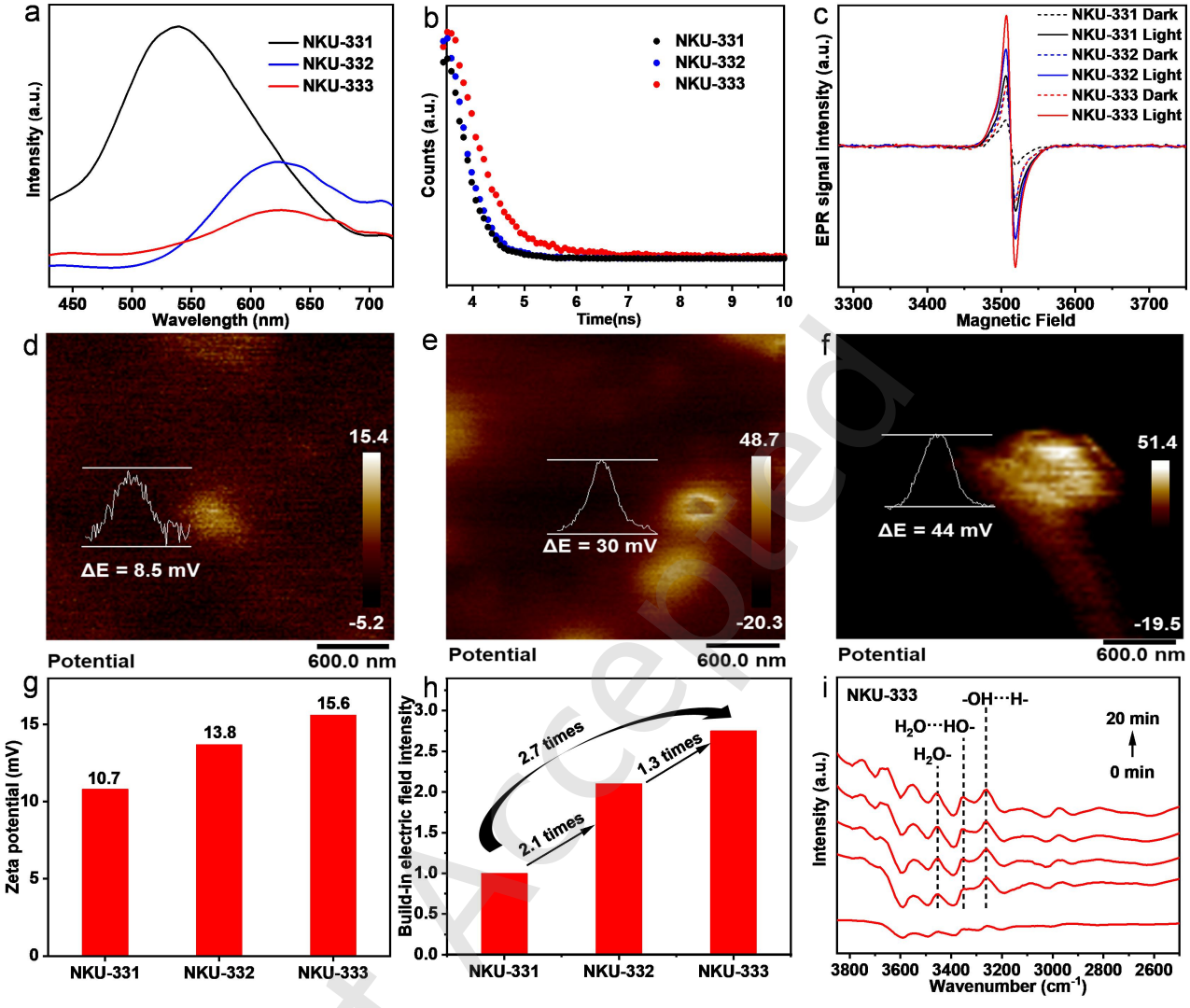

Figure 4. (a) Steady-state and (b) Time-resolved PL spectra of NKU-331–333 (λ_{ex} = 300 nm). (c) EPR spectra of NKU-331–333 in the dark and light. Surface potentials via KPFM for (d) NKU-331, (e) NKU-332 and (f) NKU-333. (g) The zeta potentials of NKU-331–333. (h) Normalized BIEF strength of NKU-331–333. (i) In situ DRIFTS monitored water molecule adsorption of NKU-333.

relatively lower recombination rate of photogenerated carriers [51, 56]. Time-resolved photoluminescence spectra showed that NKU-333 had the longest lifetime of 0.46 ns among the three COFs (Figure 4b and Table S2), indicating a prolonged excited-state lifetime that is conducive to charge separation. The charge separation dynamics of NKU-331–333 were investigated through electron paramagnetic resonance (EPR) spectra (Fig. (4c)). NKU-331–333 exhibited markedly intensified EPR signals upon illumination, verifying the effective production of photoinduced electron-hole pairs. Under the same conditions, the EPR intensity of NKU-333 is higher than NKU-331 and NKU-332, suggesting that NKU-333 had better charge separation efficiency. NKU-333 exhibited the weakest PL emission, the longest excited-state lifetime, and the strongest light-induced EPR signal, confirming its most effective suppression of electron-hole recombination as well as superior charge separation capability.

The BIEF is an electrostatic field spontaneously formed due to inhomogeneous charge distribution, which can promote the separation and transport of charge carriers to influence the photocatalytic activity [18]. Kelvin probe force microscopy (KPFM) measurements were performed to investigate the surface potential of NKU-331–333 (Figs. (4d)–(4f)). The surface potentials of NKU-331, NKU-332 and NKU-333 were 8.5 mV, 30 mV and 44 mV, respectively. The surface potential of NKU-333 was significantly higher than those of NKU-332 and NKU-331. The zeta potentials of NKU-331, NKU-332 and NKU-333 were 10.7, 13.8 and 15.6 mV, respectively (Figs. (4g) and (S20)). The BIEF of a material has a monotonic positive correlation with both surface potential and zeta potential [17–20]. By combining the surface potential with the zeta potential, the BIEF strength of NKU-333 was 1.3 times that of NKU-332 and 2.7 times that of NKU-331 (Fig. (4h)). These results further confirm that the suitable donor-acceptor arrangement in NKU-333 provides a strong BIEF to promote the separation and transport of photogenerated charge carriers for enhancing

Just Accepted

photocatalytic hydrogen evolution activity. The water molecule adsorption kinetics

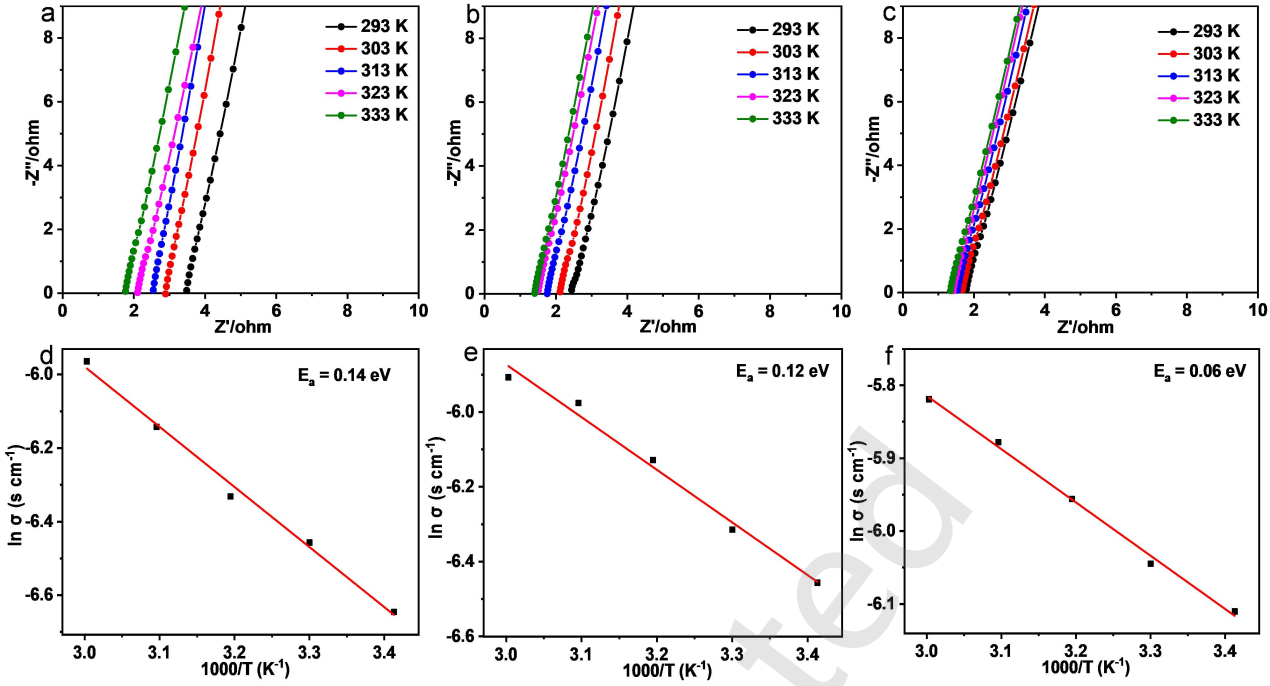

Figure 5. Temperature-dependent proton conductivity of NKU-331 (a), NKU-332 (b), and NKU-333 (c) at 99% relative humidity, and the Arrhenius plots of NKU-331 (d), NKU-332 (e), and NKU-333 (f).

within NKU-331–333 were monitored using in-situ diffuse reflectance infrared Fourier transform spectroscopy (DRIFTS) (Figs. (4i), (S21) and (S22)). With water vapor, the peaks in 3558-3250 cm^{-1} from adsorbed water molecules could be observed. Specifically, the peak at 3558 cm^{-1} is attributed to O–H stretching vibrations of H_2O molecules, while the peak at 3460 cm^{-1} originates from intermolecular hydrogen bonding [26]. The peak at 3250 cm^{-1} corresponds to coupled symmetric/asymmetric O–H stretching modes of water molecules [12]. This result demonstrates the water adsorption potentials of NKU-331–333.

Proton conductivity of photocatalysts plays a key role in photocatalytic hydrogen evolution [37, 66]. NKU-331–333 exhibit proton conductivities of 1.30, 1.57 and 2.27 mS cm^{-1} at room temperature and 99% relative humidity, respectively. The proton conductivities of NKU-331–333 gradually increase with increasing temperature, eventually reaching maximum values of 2.57, 2.72, and 2.97 mS cm^{-1} at 333 K, respectively (Figs. (5a)–(5c) and (S23)–(S25)), which are competitive with most COFs under humid conditions (Table S3). Based on the temperature-dependent proton conductivities, the activation energy (E_a) is 0.06 eV for NKU-333, lower than 0.12 eV of NKU-332 and 0.14 eV of NKU-331 (Figs. (5d)–(5f)). The efficient proton transfer and the low activation energy are both beneficial for promoting the photocatalytic activities.

The exciton binding energy (E_b) critically governs the photocatalytic performance by influencing exciton dissociation efficiency and charge recombination dynamics [73]. Temperature-dependent PL spectra were measured. The PL intensities of the three COFs gradually decrease with increasing temperature (Figs. (S26)–(S28)), which is predominantly ascribed to thermally activated nonradiative recombination pathway [74, 75]. The E_b values of NKU-331, NKU-332, and NKU-333 were determined by fitting the experimental data, to give 43.9, 39.8, and 34.1 meV, respectively. The lowest E_b value of NKU-333 indicates that the enhanced BIEF facilitates exciton dissociation, increases the number of free charge carriers, and thus boosts the photocatalytic activity.

To elucidate the reaction mechanism and further understand the origin of the superior photocatalytic activity of NKU-333, the electronic structures of these COFs were studied by high-level density functional theory (DFT) calculations. The lowest unoccupied molecular orbital (LUMO) of all COFs were localized on the guanidine units (Fig. 6). However, the highest occupied molecular orbital (HOMO) distributions exhibited distinct differences. The HOMO location of NKU-331 is spread on the benzene unit and guanidine units. In contrast, the HOMO positions of NKU-332 and NKU-333 are solely centered on the pyridine and bipyridine units. This D–A arrangement directly forms a BIEF from the donor to the acceptor. The spatial separation of HOMO and LUMO minimizes the overlap between photogenerated electrons and holes in NKU-332 and NKU-333, thereby suppressing their recombination. Combined with electrostatic potential (ESP) calculations and the calculated dipole moments, the well-defined D–A arrangement in NKU-333 is more favorable for forming a strong BIEF compared to NKU-331/332, thereby effectively promoting charge separation and carrier migration, to achieve the superior photocatalytic activity.

Just Accepted

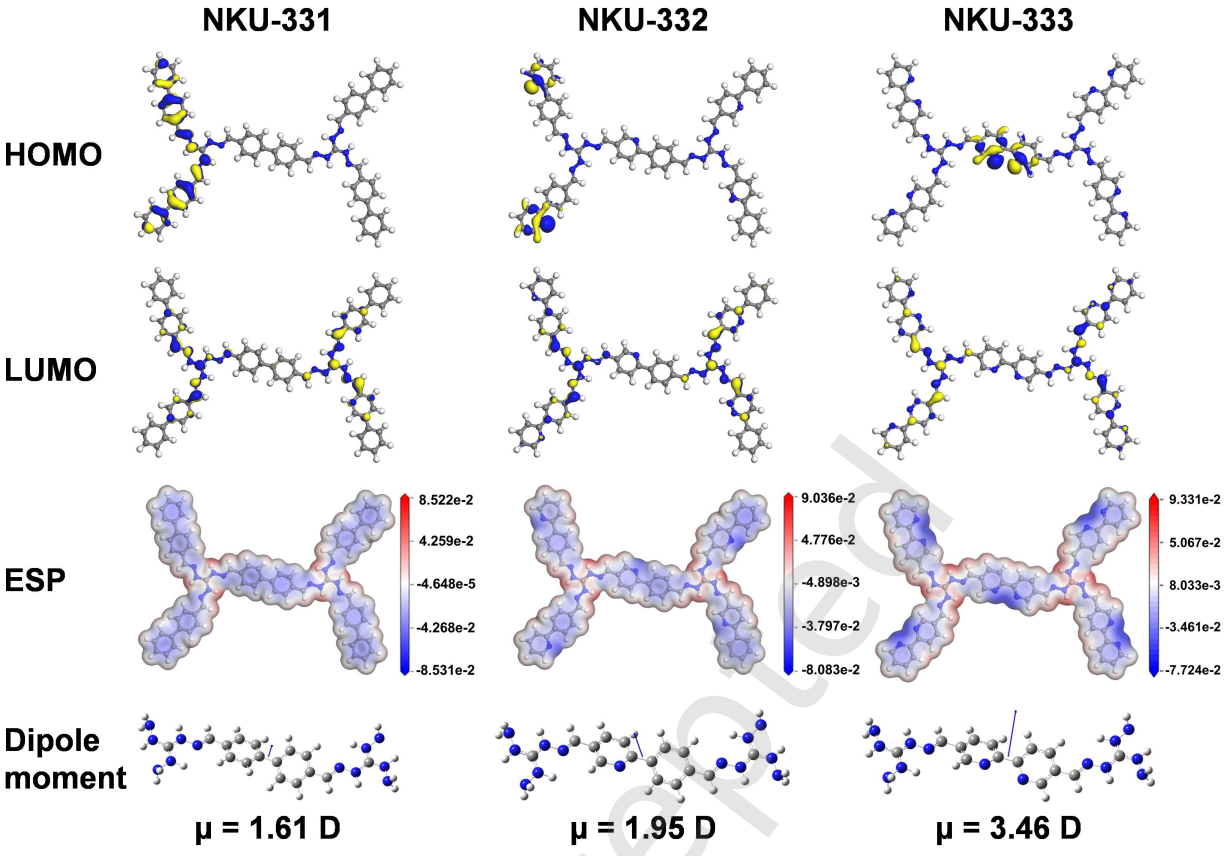

Figure 6. The HOMO and LUMO orbitals, the molecular electrostatic potentials, and the dipole moments of NKU-331–333.

4. Conclusions

In summary, three D–A-based COFs were synthesized in gram scale via a facile one-pot reaction using ethanol as the solvent and were employed as effective photocatalysts for hydrogen evolution. The BIEF was finely regulated by modifying the donor units without changing their main structures, resulting in a significantly increased hydrogen production rate from 2.3 to 31.8 mmol g^{-1} h^{-1}. This enhancement is attributed to the markedly improved charge separation efficiency and superior charge separation and transport ability driven by the strong BIEF in NKU-333. Importantly, the crucial role of the enhanced BIEF by the well-arranged D–A component in COFs was revealed, providing valuable insight for designing high-performance photocatalysts.

Electronic Supplementary Material:
Supplementary material (please give brief details, e.g., further details of the annealing and oxidation procedures, STM measurements, AFM imaging and Raman spectroscopy measurements) is available in the online version of this article at https://doi.org/10.26599/NR.2026.94909327.

Data availability

The data that support the findings of this study are available in the Supporting Information of this article.

Acknowledgements

This research was funded by the National Natural Science Foundation of China (Grant Nos. 22121005, 92572108 and 22471128), the "111 Center" (Grant Nos. B25010 and B26005) and the Fundamental Research Funds for the Central Universities (Grant No. 63261001).

Declaration of competing interest

The authors declare no competing interests.

Author contribution statement

M. X.: Data curation, methodology, validation, writing manuscript, experimental design. P. D. L., W. H. H., and S. Q. Z.: Data curation, validation, experimental design. J. X. and Z. Z.: Data curation. P. C.: Project administration, funding acquisition. W. S.: Project administration, methodology, funding acquisition, writing manuscript. All the authors have approved the final manuscript.

Use of AI statement

None.

References

[1] Zhou, P.; Navid, I. A.; Ma, Y. J.; Xiao, Y.; Wang, P.; Ye, Z.; Zhou, B.; Sun, K.; Mi, Z. Solar-to-hydrogen efficiency of more than 9% in photocatalytic water splitting. *Nature* **2023**, *613*, 66–70.

[2] Zhang, S.; Lu, L.; Jiang, J.; Liu, N.; Zhao, B.; Xu, M.; Cheng, P.; Shi, W. Organizing photosensitive and photothermal single-sites uniformly in a trimetallic metal–organic framework for efficient photocatalytic hydrogen evolution. *Adv. Mater.* **2024**, *36*, 2403464.

[3] He, S.; Chen, Y.; Fang, J.; Liu, Y.; Lin, Z. Optimizing photocatalysis via electron spin control. *Chem. Soc. Rev.* **2025**, *54*, 2154–2187.

[4] Wang, Z.; Ding, G.; Li, C.; Huang, H.; Xiao, Y.; Chen, Z.; Zhang, J.; Xiao,

Just Accepted

H.; Wang, Z.; Chen, L.; Shuai, L.; Ni, Y.; Liao, G. Hydrogen-bonds bridged biomass-assisted S-scheme junction boosts proton-coupled electron transfer for H_2O_2 photosynthesis. *eScience* **2026**, *6*, 100562.

[5] Lan, W.; Gou, X.; Wu, Y.; Liu, N.; Lu, L.; Cheng, P.; Shi, W. The influence of light-generated radicals for highly efficient solar-thermal conversion in an ultra-stable 2D metal-organic assembly. *Angew. Chem. Int. Ed*. **2024**, *63*, e202401766.

[6] Zhao, X.; Zhang, Z.; Li, C.; Liu, L.; Xiao, Y.; Wang, Z.; Li, S.; Soo, H. S. Steering the adsorption modes and oxidation state of Co oxyhydroxide active sites to unlock selective glucose oxidation to formate for efficient solar reforming of biomass to green hydrogen. *eScience* **2025**, *5*, 100431.

[7] Han, Z.; Zhang, R.; Jiang, J.; Chen, Z.; Ni, Y.; Xie, W.; Xu, J.; Zhou, Z.; Chen, J.; Cheng, P.; Shi, W. High-efficiency lithium-ion transport in a porous coordination chain-based hydrogen-bonded framework. *J. Am. Chem. Soc*. **2023**, *145*, 10149–10158.

[8] Zhang, R.; Lu, L.; Cheng, P.; Shi, W. Bimetallic MOF-based catalysts with enhanced activity for electrochemical hydrogen evolution in acid and alkaline electrolytes. *Inorg. Chem. Front.* **2024**, *11*, 7492–7500.

[9] Nishiyama, H.; Yamada, T.; Nakabayashi, M.; Maehara, Y.; Yamaguchi, M.; Kuromiya, Y.; Nagatsuma, Y.; Tokudome, H.; Akiyama, S.; Watanabe, T.; Narushima, R.; Okunaka, S.; Shibata, N.; Takata, T.; Hisatomi, T.; Domen, K. Photocatalytic solar hydrogen production from water on a 100-m^2 scale. *Nature* **2021**, *598*, 304–307.

[10] Liu, N.; Jiang, J.; Chen, Z.; Wu, B.; Zhang, S.; Zhang, Y.-Q.; Cheng, P.; Shi, W. Promoted photocatalytic hydrogen evolution by tuning the electronic state of copper sites in metal-organic supramolecular assemblies. *Angew. Chem. Int. Ed*. **2023**, *62*, e202312306.

[11] Zhang, R.; Chen, Z.; Jiang, J.; Liao, X.; Guo, J.; Huang, W.; Liu, J.; Dang, S.; Xu, J.; Wang, H.; Zhou, Z.; Zhang, K.; Cheng, P.; Shi, W. Ordered lithiophilic crown ether sites in a two-dimensional coordination network for dendrite-free lithium deposition. *CCS Chem*. **2025**, *7*, 3160–3171.

[12] Wang, J.; Zhang, Y.; Jiang, S.; Sun, C.; Song, S. Regulation of d-band centers in localized CdS homojunctions through facet control for improved photocatalytic water splitting. *Angew. Chem. Int. Ed*. **2023**, *62*, e202307808.

[13] Yuan, A.; Liu, H.; Wang, H.; He, T.; Zhang, H.; Hu, D.; Li, Y.; An, D.; Ma, L.; Chen, S.; Chen, L. Lattice oxygen mechanism triggered via stable Ni–O–W for solar-boosted water electrolysis. *eScience* **2026**, *6*, 100533.

[14] Li, H.; Fan, J.; Ran, M.; Borse, R. A.; Lin, S.-X.; Yuan, D. Design and construction of D–A-extended 3D covalent organic frameworks for boosting photocatalytic hydrogen evolution. *Angew. Chem. Int. Ed*. **2025**, *64*, e202500937.

[15] Kosco, J.; Gonzalez-Carrero, S.; Howells, C. T.; Fei, T.; Dong, Y.; Sougrat, R.; Harrison, G. T.; Firdaus, Y.; Sheelamanthula, R.; Purushothaman, B.; Moruzzi, F.; Xu, W.; Zhao, L.; Basu, A.; De Wolf, S.; Anthopoulos, T. D.; Durrant, J. R.; McCulloch, I. Generation of long-lived charges in organic semiconductor heterojunction nanoparticles for efficient photocatalytic hydrogen evolution. *Nat. Energy* **2022**, *7*, 340–351.

[16] Kosco, J.; Bidwell, M.; Cha, H.; Martin, T.; Howells, C. T.; Sachs, M.; Anjum, D. H.; Gonzalez Lopez, S.; Zou, L.; Wadsworth, A.; Zhang, W.; Zhang, L.; Tellam, J.; Sougrat, R.; Laquai, F.; DeLongchamp, D. M.; Durrant, J. R.; McCulloch, I. Enhanced photocatalytic hydrogen evolution from organic semiconductor heterojunction nanoparticles. *Nat. Mater*. **2020**, *19*, 559–565.

[17] Sheng, Y.; Li, W.; Xu, L.; Zhu, Y. High photocatalytic oxygen evolution via strong built-in electric field induced by high crystallinity of perylene imide supramolecule. *Adv. Mater.* 2022, *34*, 2102354.

[18] Shen, R.; Huang, C.; Hao, L.; Liang, G.; Zhang, P.; Yue, Q.; Li, X. Ground-state charge transfer in single-molecule junction covalent organic frameworks for boosting photocatalytic hydrogen evolution. Nat. Commun. 2025, 16, 2457.

[19] Yu, Y.; Yan, W.; Wang, X.; Li, P.; Gao, W.; Zou, H.; Wu, S.; Ding, K. Surface engineering for extremely enhanced charge separation and photocatalytic hydrogen evolution on g-C_3N_4. *Adv. Mater*. **2018**, *30*, 1705060.

[20] Li, J.; Cai, L.; Shang, J.; Yu, Y.; Zhang, L. Giant enhancement of internal electric field boosting bulk charge separation for photocatalysis. *Adv. Mater*. **2016**, *28*, 4059–4064.

[21] Yin, Y.; Zhang, Y.; Zhou, X.; Gui, B.; Wang, W.; Jiang, W.; Zhang, Y.-B.; Sun, J.; Wang, C. Ultrahigh-surface area covalent organic frameworks for methane adsorption. *Science* **2024**, *386*, 693–696.

[22] Liu, W.; Liu, Z.; Gong, L.; Wang, K.; Wu, B.; Jiang, J. Integrating urea-based units into porphyrinic covalent organic framework for efficient artemisinin photosynthesis. *Angew. Chem. Int. Ed*. **2025**, *64*, e202506462.

[23] Chang, J.; Zhang, Z.; Zheng, H.; Li, H.; Suo, J.; Ji, C.; Chen, F.; Zhang, S.; Wang, Z.; Valtchev, V.; Qiu, S.; Sun, J.; Fang, Q. Synthesis of three-dimensional covalent organic frameworks through a symmetry reduction strategy. *Nat. Chem*. **2025**, *17*, 571–581.

[24] Zhao, W.; Zhu, Q.; Wu, X.; Zhao, D. The development of catalysts and auxiliaries for the synthesis of covalent organic frameworks. *Chem. Soc. Rev.* **2024**, *53*, 7531–7565.

[25] He, Z.; Liu, C.; Yu, T.; Xu, J.; Thériault, P.; Gohari, M.; Ruchlin, C.; Che, Y.; Titi, H.; Ghamari, P.; Kena-Cohen, S.; Perepichka, D. Merocyanine-linked zwitterionic covalent organic frameworks. *J. Am. Chem. Soc.* **2026**, *148*, 640–649.

[26] Qu, J.-D.; Wang, Y.; Sun, T.-T.; Chu, X.-Y.; Jiang, Y.-X.; Zhang, N.-N.; Zhao, Z.-H.; Dong, H.; Lan, Y.-Q.; Zhang, F.-M. Engineering covalent organic frameworks for photocatalytic overall water vapor splitting. *Angew. Chem. Int. Ed.* **2025**, 64, e202502821.

[27] Wu, X.; Guo, J.; Sun, M.; Du, T.; Hao, D.; Liu, D.; Wang, D.; Wen, S.; Yin, J.; Li, D.; He, J. Construction of heteroleptic copper complexes in perylene diimide-based COFs for heterogeneous metallaphotoredox catalysis. *J. Am. Chem. Soc.* **2026**, *148*, 4283–4294.

[28] Rath, B. B.; Lotsch, B. V. Ion diffusion and (photo)redox conductivity in a covalent organic framework. *J. Am. Chem. Soc.* **2026**, *148*, 3305–3315.

[29] Zuo, Q.; Chu, B.; Ye, X.; Li, F.; Li, L.; Xu, Q. Enzyme-click postsynthetic modification of covalent organic frameworks for photocatalytic H_2O_2 production. *J. Am. Chem. Soc.* **2025**, *147*, 34681–34689.

[30] Qin, W.; Jin, Y.; Zhang, L.; Wang, C.; Sun, J.; Tung, C.; Wu, L. Topology-optimized 3D metalloporphyrin covalent organic framework for photocatalytic CO_2 fixation. *J. Am. Chem. Soc.* **2025**, *147*, 33066–33070.

[31] Shao, P.; Ren, Z.; Zhao, B.; Wang, X.; Li, J.; Xie, J.; Wang, B.; Feng, X. Theory-guided design of N-confused porphyrinic covalent organic frameworks for oxygen reduction reaction. *J. Am. Chem. Soc*. **2025**, *147*, 8769–8777.

[32] Zhang, Z.; Liu, Y.; Qi, Y.; Yu, Z.; Chen, X.; Li, C.; Shi, Z.; Feng, S. Self-catalysis acceleration of carrier transport in one-dimensional covalent organic frameworks with mortise-tenon stacking. *Angew. Chem. Int. Ed.* **2025**, *64*, e202501614.

[33] Wang, W.-Z.; Tian, P.-J.; Fu, Y.; Wan, X.-L.; Lei, X.; Jia, C.; Liu, C.; Qi, Q.-Y.; Xu, S.-Q.; Zhao, X. Orthorhombic covalent organic frameworks with fmj topology as photocatalyst for hydrogen evolution. *Angew. Chem. Int. Ed*. **2025**, *64*, e202418086.

[34] Arora, N.; Flores, C.; Senarathna, M. C.; Thompson, C. M.; Smaldone, R. A. Design, synthesis, and applications of mesoporous covalent organic frameworks. *CCS Chem*. **2024**, *6*, 57–68.

[35] Xu, J.; Li, W.; Liu, W.; Jing, J.; Zhang, K.; Liu, L.; Yang, J.; Zhu, E.; Li, J.; Zhu, Y. Efficient photocatalytic hydrogen and oxygen evolution by side-group engineered benzodiimidazole oligomers with strong built-in electric fields and short-range crystallinity. *Angew. Chem. Int. Ed*. **2022**, *61*, e202212243.

[36] Zhang, Y.; Li, Y.; Xin, X.; Wang, Y.; Guo, P.; Wang, R.; Wang, B.; Huang, W.; Sobrido, A. J.; Li, X. Internal quantum efficiency higher than 100% achieved by combining doping and quantum effects for photocatalytic overall water splitting. *Nat. Energy* **2023**, *8*, 504–514.

[37] Liu, N.; Jiang, J.; Zhang, S.; Zhang, R.; Xu, M.; Chen, Z.; Cheng, P.; Shi, W. Arrangement of ordered D–A components in a metal-organic framework for cocatalyst-free photocatalytic hydrogen evolution with efficient proton conduction. *Angew. Chem. Int. Ed*. **2025**, *64*, e202501141.

[38] Yang, J.; Jing, J.; Zhu, Y. A full-spectrum porphyrin–fullerene D–A supramolecular photocatalyst with giant built-in electric field for efficient hydrogen production. *Adv. Mater*. **2021**, *33*, 2101026.

[39] Chu, X.; Liu, S.; Luan, B.-B.; Zhang, Y.; Xi, Y.; Shao, L.-H.; Zhang, F.-M.; Lan, Y.-Q. Crystal-facet-controlled internal electric field in MOF/COF heterojunction towards efficient photocatalytic overall water splitting. *Angew. Chem. Int. Ed*. **2025**, *64*, e202422940.

[40] Zhang, H.; Lin, Z.; Kidkhunthod, P.; Guo, J. Stable immobilization of nickel ions on covalent organic frameworks for panchromatic photocatalytic hydrogen evolution. *Angew. Chem. Int. Ed*. **2023**, *62*, e202217527.

[41] Zou, L.; Si, D.; Yang, S.; Chen, Z.; Huang, Y.; Cao, R. Induced charge-compensation effect for boosting photocatalytic water splitting in covalent organic frameworks. *Angew. Chem. Int. Ed.* **2025**, *64*, e202418319.

[42] Luo, Z.; Zhu, S.; Xue, H.; Yang, W.; Zhang, F.; Xu, F.; Lin, W.; Wang, H.;

Just Accepted

Chen, X. Manipulating p–π resonance through methoxy group engineering in covalent organic frameworks for an efficient photocatalytic hydrogen evolution. *Angew. Chem. Int. Ed.* **2025**, *64*, e202420217.

[43] Wang, Y.; Qiao, Z.; Li, H.; Zhang, R.; Xiang, Z.; Cao, D.; Wang, S. Molecular engineering for modulating photocatalytic hydrogen evolution of fully conjugated 3D covalent organic frameworks. *Angew. Chem. Int. Ed.* **2024**, *63*, e202404726.

[44] Zhang, Z.; Xu, Y. Hydrothermal synthesis of highly crystalline zwitterionic vinylene-linked covalent organic frameworks with exceptional photocatalytic properties. *J. Am. Chem. Soc.* **2023**, *145*, 25222–25232.

[45] Cheng, J.; Wu, Y.; Zhang, W.; Zhang, J.; Wang, L.; Zhou, M.; Fan, F.; Wu, X.; Xu, H. Fully conjugated 2D sp^2 carbon-linked covalent organic frameworks for photocatalytic overall water splitting. *Adv. Mater.* **2024**, *36*, 2305313.

[46] Dong, W.; Qin, Z.; Wang, K.; Xiao, Y.; Liu, X.; Ren, S.; Li, L. Isomeric Oligo(phenylenevinylene)-based covalent organic frameworks with different orientation of imine bonds and distinct photocatalytic activities. *Angew. Chem. Int. Ed.* **2023**, *62*, e202216073.

[47] Yao, L.; Liu, S.; Li, L.; Ge, B.; Jiao, W.; Zong, S.; Song, X.; Zhou, D.; Liang, Z. Enhancing the efficiency and durability of perovskite solar cells by donor–acceptor covalent organic framework with thiazolo[5,4-d] thiazole unit. *CCS Chem.* **2024**, *6*, 1721–1730.

[48] Manzoor, S.; Younis, M. A.; Yao, Y.; Tariq, Q.; Zhang, B.; Tian, B.; Yan, L.; Qiu, C. Schiff base COFs for photocatalysis: From fundamentals to applications. *Coord. Chem. Rev.* **2025**, *541*, 216840.

[49] Chen, J.; Yan, S.; Wang, F.; Lin, F.; Lin, J.; Borse, R. A.; Wang, Y. Redox-mediated TEMPO-based donor-acceptor covalent organic framework for efficient photo-induced hydrogen peroxide generation. *Angew. Chem. Int. Ed.* **2025**, *64*, e202500924.

[50] Li, B.; Chen, J.; Dong, W.; Gong, L.; Yang, T.; Wang, K.; Qi, D.; Wang, T.; Jiang, J. Lattice strain in multi-component covalent organic frameworks for enhanced H_2O_2 photosynthesis. *Angew. Chem. Int. Ed.* **2026**, *65*, e19444.

[51] Xu, H.; Xia, S.; Li, C.; Li, Y.; Xing, W.; Jiang, Y.; Chen, X. Programming tetrathiafulvalene-based covalent organic frameworks for promoted photoinduced molecular oxygen activation. *Angew. Chem. Int. Ed.* **2024**, *63*, e202405476.

[52] Yang, H.; Hao, M.; Xie, Y.; Liu, X.; Liu, Y.; Chen, Z.; Wang, X.; Waterhouse, G. I. N.; Ma, S. Tuning local charge distribution in multicomponent covalent organic frameworks for dramatically enhanced photocatalytic uranium extraction. *Angew. Chem. Int. Ed.* **2023**, *62*, e202303129.

[53] Yang, J.; Acharjya, A.; Ye, M.; Rabeah, J.; Li, S.; Kochovski, Z.; Youk, S.; Roeser, J.; Grüneberg, J.; Penschke, C.; Schwarze, M.; Wang, T.; Lu, Y.; van de Krol, R.; Oschatz, M.; Schomäcker, R.; Saalfrank, P.; Thomas, A. Protonated imine-linked covalent organic frameworks for photocatalytic hydrogen evolution. *Angew. Chem. Int. Ed.* **2021**, *60*, 19797–19803.

[54] Wang, Y.; Hao, W.; Liu, H.; Chen, R.; Pan, Q.; Li, Z.; Zhao, Y. Facile construction of fully sp^2-carbon conjugated two-dimensional covalent organic frameworks containing benzobisthiazole units. *Nat. Commun.* **2022**, *13*, 100.

[55] Zhang, H.; Ba, D.; Zou, C.; Cheng, L.; Cheng, S.; Dong, W.; Zhao, J.; Li, D. Acceptor strength modulates keto-enol tautomerism in donor–acceptor COFs for enhanced photocatalytic aerobic oxidation. *Angew. Chem. Int. Ed.* **2026**, *65*, e19829.

[56] Liu, C.; Liu, X.; Chen, B.; Li, Z.; Ou, X.; Lu, Y.; Liu, Y.; Wu, C.; Yao, S.; Liu, Y.; Ye, L.; Han, B.; Yang, Z. Squaric acid-based zwitterionic covalent organic framework induces triple synergy for boosted hydrogen peroxide photosynthesis. *Nat. Commun.* **2025**, *16*, 8941.

[57] Liu, Y.; Deng, X.; Wang, Z.; Yin, S.; Chen, P. Gradient polarization induces three-dimensional asymmetric electron distribution in covalent organic frameworks for dramatically enhanced photocatalytic overall nitrogen fixation. *Angew. Chem. Int. Ed.* **2025**, *64*, e202516117.

[58] Zhang, J.; Xue, F.; Wang, Z. Terpyridine- and quarterpyridine-based cationic covalent organic frameworks for visible-light-catalytic H_2O_2 synthesis. *Angew. Chem. Int. Ed.* **2025**, *64*, e202425617.

[59] Wang, K.; Zhong, Y.; Dong, W.; Xiao, Y.; Ren, S.; Li, L. Intermediate formation of macrocycles for efficient crystallization of 2D covalent organic frameworks with enhanced photocatalytic hydrogen evolution. *Angew. Chem. Int. Ed.* **2023**, *62*, e202304611.

[60] Jin, F.; Wang, T.; Han, Z.; Lin, E.; Zheng, Y.; Hao, L.; Wang, T.; Chen, Y.; Cheng, P.; Yu, K.; Zhang, Z. Bottom-up synthesis of covalent organic frameworks with quasi-three-dimensional integrated architecture via interlayer cross-linking. *J. Am. Chem. Soc.* **2023**, *145*, 6505–6515.

[61] Qin, L.; Sun, D.; Ma, D.; Wang, Z.; Liu, Y.; Li, Q.; Song, F.; Wu, K.; Gan, L.; Zhou, T.; Zhang, J. Decoupling interlayer interactions boosts charge separation in covalent organic frameworks for high-efficiency photocatalytic CO_2 reduction. *Adv. Mater.* **2025**, *37*, 2504205.

[62] Nguyen, H. L.; Gropp, C.; Ma, Y.; Zhu, C.; Yaghi, O. M. 3D covalent organic frameworks selectively crystallized through conformational design. *J. Am. Chem. Soc.* **2020**, *142*, 20335–20339.

[63] Llauradó-Capdevila, G.; Veciana, A.; Guarducci, M. A.; Mayoral, A.; Pons, R.; Hertle, L.; Ye, H.; Mao, M.; Sevim, S.; Rodríguez-San-Miguel, D.; Sorrenti, A.; Jang, B.; Wang, Z.; Chen, X.; Nelson, B. J.; Matheu, R.; Franco, C.; Pané, S.; Puigmartí-Luis, J. Tailored design of a water-based nanoreactor technology for producing processable sub-40 nm 3D COF nanoparticles at atmospheric conditions. *Adv. Mater.* **2024**, *36*, 2306345.

[64] Das, G.; Garai, B.; Prakasam, T.; Benyettou, F.; Varghese, S.; Sharma, S. K.; Gándara, F.; Pasricha, R.; Baias, M.; Jagannathan, R.; Saleh, N.; Elhabiri, M.; Olson, M. A.; Trabolsi, A. Fluorescence turn on amine detection in a cationic covalent organic framework. *Nat. Commun.* **2022**, *13*, 3904.

[65] Zhang, Z.; Dong, X.; Jin, Y.; Liu, Z.; Li, X.; Zhang, D.; Pan, T.; Lei, Q.; Liu, X.; Xie, Y.; Shui, F.; Li, J.; Yi, M.; Yuan, J.; You, Z.; Zhang, L.; Chang, J.; Zhang, H.; Fang, Q.; Li, B.; Bu, X.; Han, Y. Chemically stable guanidinium covalent organic framework for the efficient capture of low-concentration iodine at high temperatures. *J. Am. Chem. Soc.* **2022**, *144*, 6821–6829.

[66] Das, G.; Shinde, D. B.; Melepurakkal, A.; Shelke, M. V.; Garai, B.; Bazin, P.; Ait Blal, A.; Benyettou, F.; Prakasam, T.; Abdul Halim, R.; Abou Ibrahim, F.; Sharma, S. K.; Varghese, S.; Weston, J.; Jagannathan, R.; Addicoat, M. A.; Gándara, F.; Olson, M. A.; El-Roz, M.; Trabolsi, A. Synergistic humidity-responsive mechanical motion and proton conductivity in a cationic covalent organic framework. *Chem* **2024**, *10*, 2500–2517.

[67] An, Q.; Zhi, S.; Zhu, H.; Liu, L.; Mao, P.; Zhao, G.; Zha, Y.; Xie, F.; Fan, Y.; Qiu, L.; Duan, L.; Guo, H. Upgrading interface chemistry via high dielectric constant and enhanced electronic localization COF for lithium metal batteries. *eScience* **2026**, 100603.

[68] Mi, Z.; Yang, P.; Wang, R.; Unruangsri, J.; Yang, W.; Wang, C.; Guo, J. Stable radical cation-containing covalent organic frameworks exhibiting remarkable structure-enhanced photothermal conversion. *J. Am. Chem. Soc.* **2019**, *141*, 14433–14442.

[69] Yang, Y.; Chu, X.; Zhang, H.; Zhang, R.; Liu, Y.; Zhang, F.; Lu, M.; Yang, Z.; Lan, Y. Engineering β-ketoamine covalent organic frameworks for photocatalytic overall water splitting. *Nat. Commun.* **2023**, *14*, 593.

[70] Ma, S.; Deng, T.; Li, Z.; Zhang, Z.; Jia, J.; Li, Q.; Wu, G.; Xia, H.; Yang, S.; Liu, X. Photocatalytic hydrogen production on a sp^2-carbon-linked covalent organic framework. *Angew. Chem. Int. Ed.* **2022**, *61*, e202208919.

[71] Peralta, R. A.; Huxley, M. T.; Evans, J. D.; Fallon, T.; Cao, H.; He, M.; Zhao, X. S.; Agnoli, S.; Sumby, C. J.; Doonan, C. J. Highly active gas phase organometallic catalysis supported within metal–organic framework pores. *J. Am. Chem. Soc.* **2020**, *142*, 13533–13543.

[72] Chen, H.; Tu, H.; Hu, C.; Liu, Y.; Dong, D.; Sun, Y.; Dai, Y.; Wang, S.; Qian, H.; Lin, Z.; Chen, L. Cationic covalent organic framework nanosheets for fast Li-ion conduction. *J. Am. Chem. Soc.* **2018**, *140*, 896–899.

[73] Chen, M.; Wang, J.; Wei, T.; Zhang, B.; Guo, K.; Feng, Y.; Zhang, B. Unprecedented flux-mediated synthesis of crystalline polyimide covalent organic frameworks using the 4-dimethylaminopyridine (DMAP)-type nucleophilic catalyst for use in efficient photosynthesis of H_2O_2. *J. Am. Chem. Soc.* **2025**, *147*, 24050–24059.

[74] Fu, G.; Yang, D.; Xu, S.; Li, S.; Zhao, Y.; Yang, H.; Wu, D.; Petkov, P. S.; Lan, Z.-A.; Wang, X.; Zhang, T. Construction of thiadiazole-bridged sp^2-carbon-conjugated covalent organic frameworks with diminished excitation binding energy toward superior photocatalysis. *J. Am. Chem. Soc.* **2024**, *146*, 1318–1325.

[75] Jia, Z.; Ji, N.; Qi, J.; Wang, T.; Che, Y.; Zhao, Z.; Zhao, J.; Jiao, Z.; Wang, K.; Zhang, W.; Zhu, W.-H. Fused-heterocycle-linked covalent organic frameworks with enhanced chemical and photochemical stability for photocatalysis. *Angew. Chem. Int. Ed.* **2025**, *64*, e202511245.

Just Accepted

Electronic Supplementary Material

Engineering built-in electric field in D–A-based covalent organic frameworks for efficient photocatalytic hydrogen evolution

Mingming Xu [1], Pengda Liu [1], Wenhao Huang [1], Shiqi Zhang [1], Jun Xu [2], Zhen Zhou [3], Peng Cheng [1], Wei Shi [1,4]

[1] Frontiers Science Center for New Organic Matter, State Key Laboratory of Advanced Chemical Power Sources and Department of Chemistry, College of Chemistry, Nankai University, Tianjin 300071, China
[2] School of Materials Science and Engineering & National Institute for Advanced Materials, Center for Rare Earth and Inorganic Functional Materials, Tianjin Key Laboratory for Rare Earth Materials and Applications, Nankai University, Tianjin 300350, China
[3] School of Materials Science and Engineering, Institute of New Energy Material Chemistry, Nankai University, Tianjin 300350, China
[4] State Key Laboratory of Elemento-Organic Chemistry, Nankai University, Tianjin 300071, China

Supporting information to https://doi.org/10.26599/NR.2026.94909327

Just Accepted

Address correspondence to Wei Shi, shiwei@nankai.edu.cn

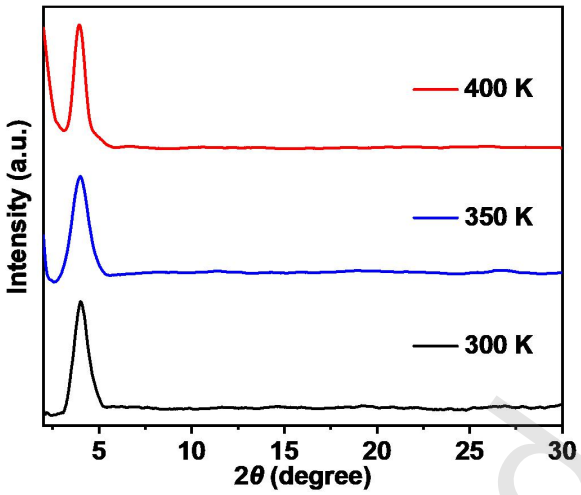

Figure S1. Temperature-dependent PXRD patterns of NKU-331.

Just Accepted

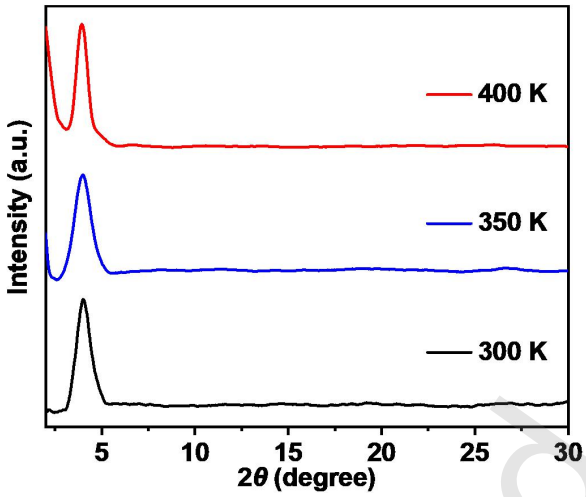

Figure S2. Temperature-dependent PXRD patterns of NKU-332.

Just Accepted

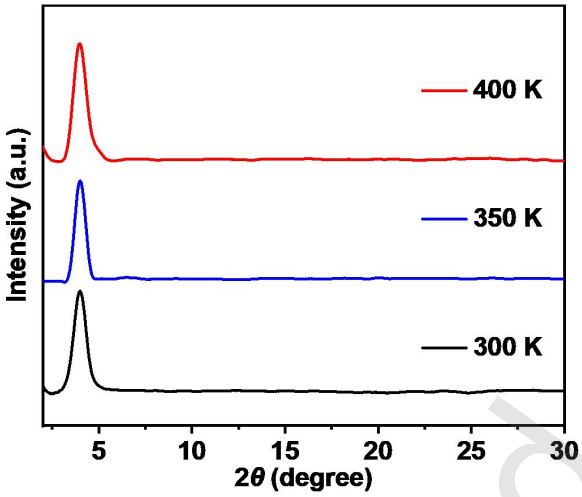

Figure S3. Temperature-dependent PXRD patterns of NKU-333.

Just Accepted

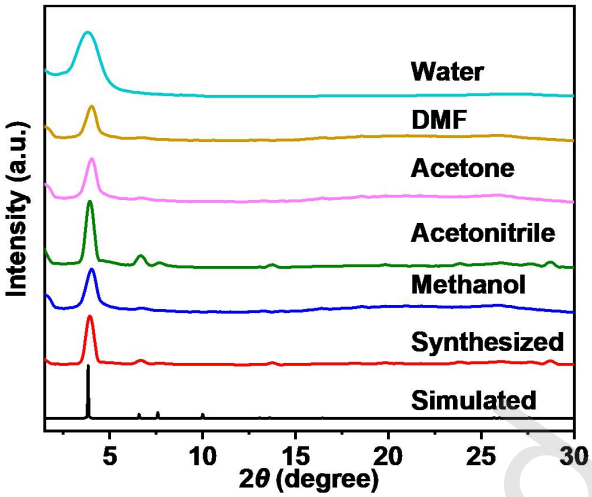

Figure S4. PXRD patterns of NKU-331 before and after immersion in different solvents.

Just Accepted

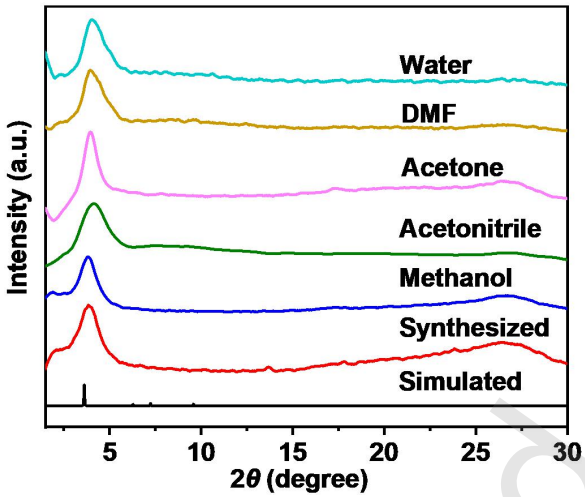

Figure S5. PXRD patterns of NKU-332 before and after immersion in different solvents.

Just Accepted

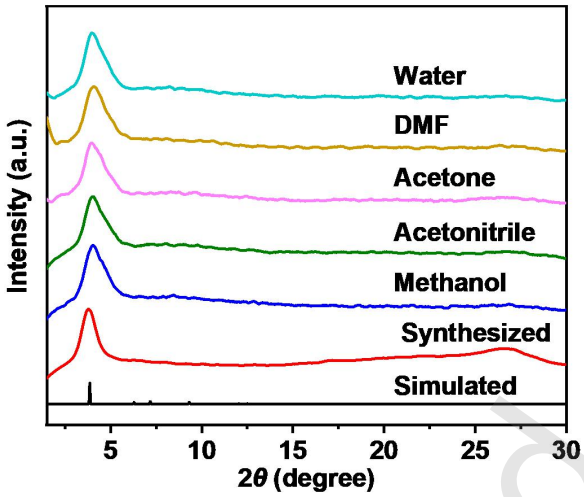

Figure S6. PXRD patterns of NKU-333 before and after immersion in different solvents.

Just Accepted

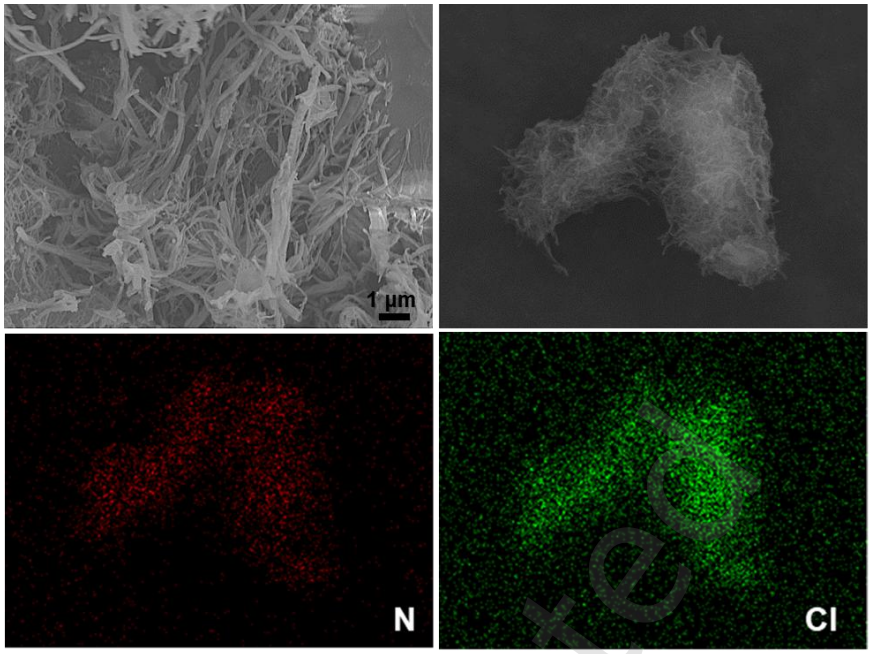

Figure S7. The SEM and EDS elemental mapping images of NKU-331.

Just Accepted

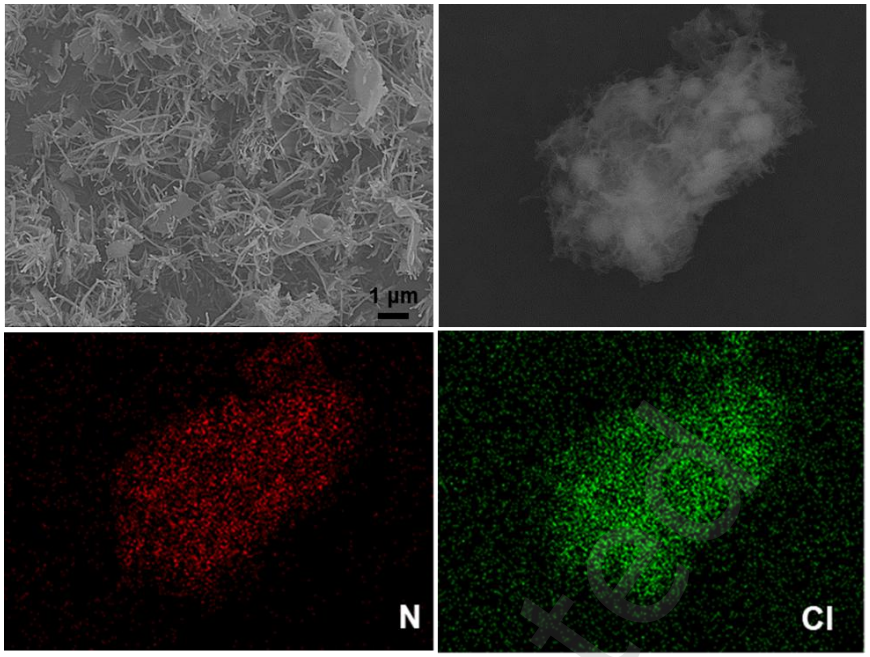

Figure S8. The SEM and EDS elemental mapping images of NKU-332.

Just Accepted

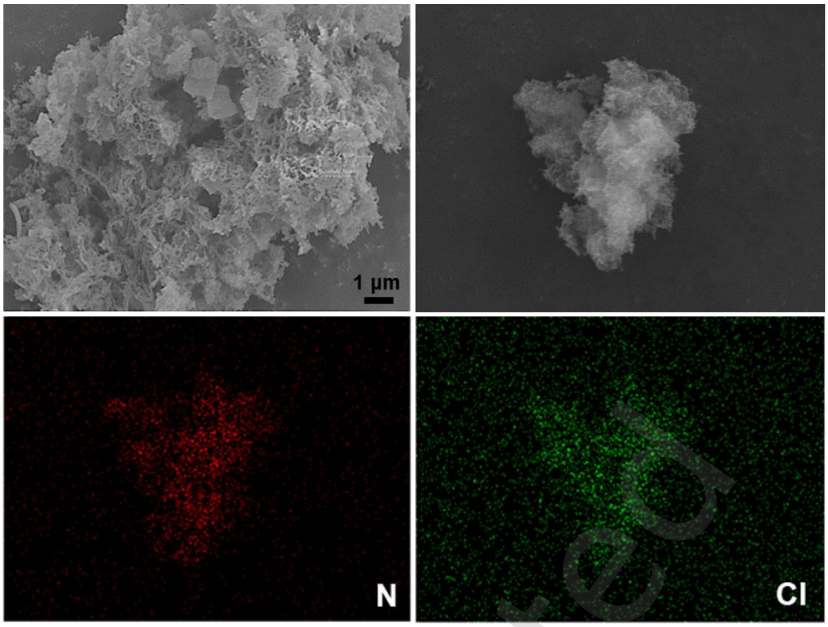

Figure S9. The SEM and EDS elemental mapping images of NKU-333.

Just Accepted

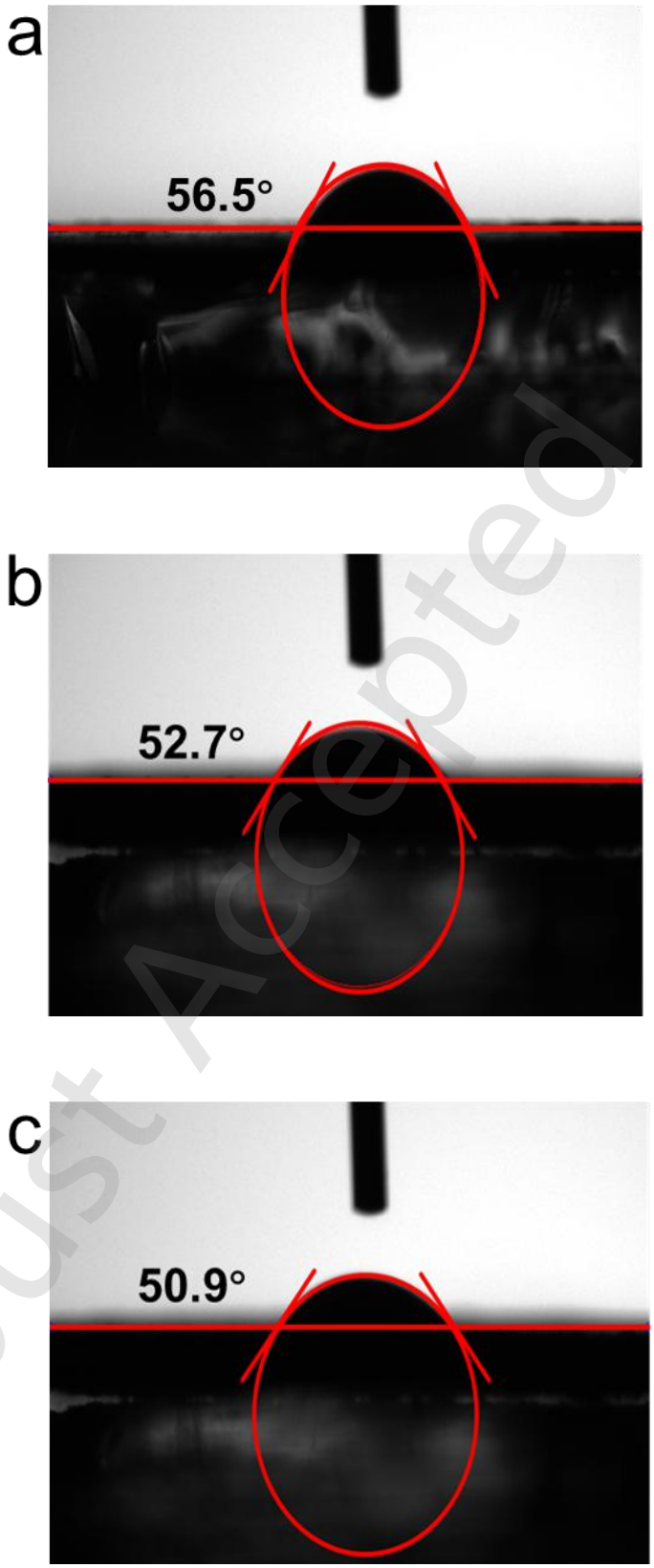

Just Accepted

Figure S10. The water contact angle images of NKU-331(a), NKU-332 (b) and NKU-333 (c).

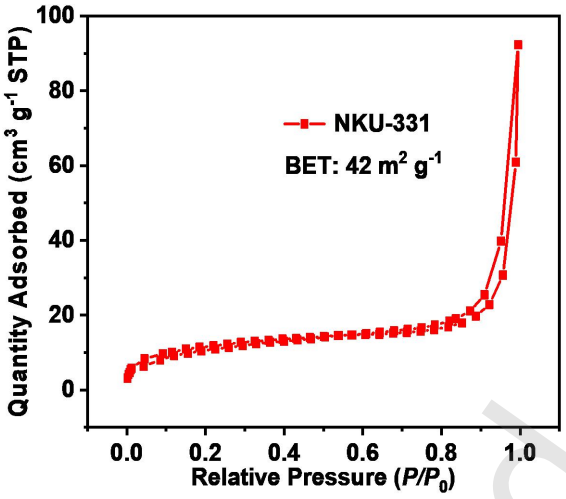

Figure S11. N_2 isotherms of NKU-331 at 77 K.

Just Accepted

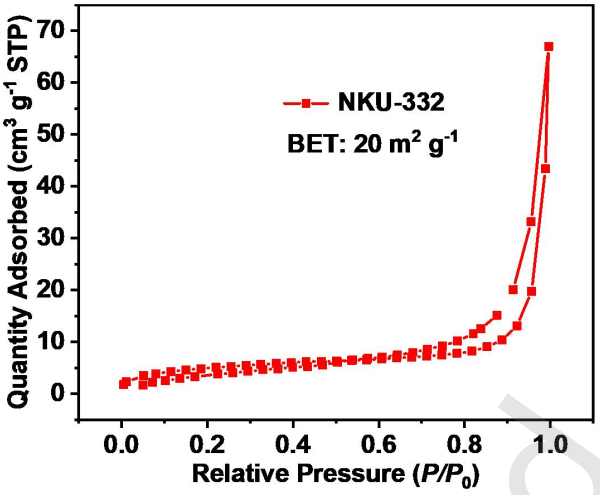

Figure S12. N_2 isotherms of NKU-332 at 77 K.

Just Accepted

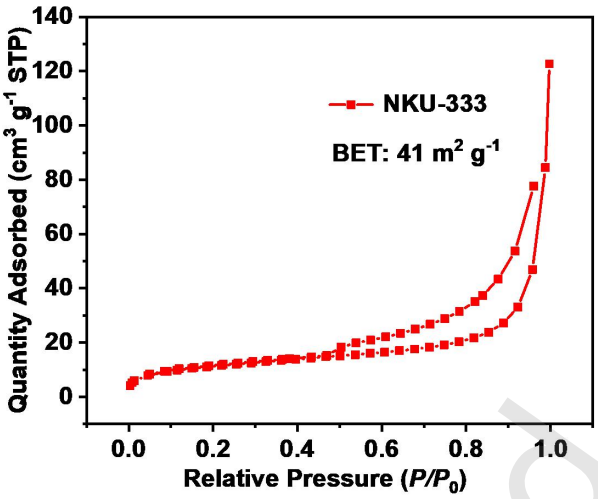

Figure S13. N_2 isotherms of NKU-333 at 77 K.

Just Accepted

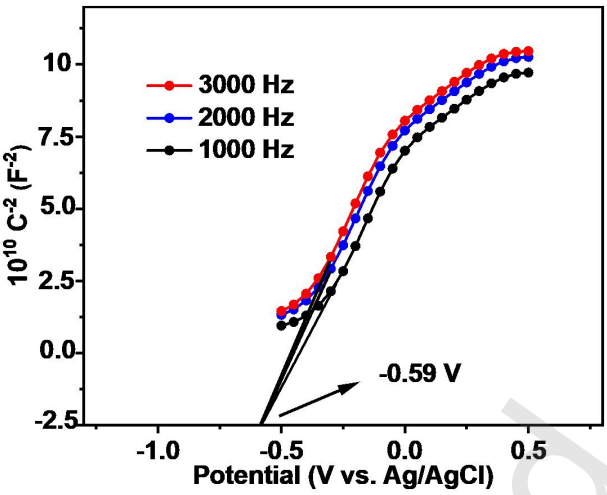

Figure S14. Mott-Schottky plots of NKU-331.

Just Accepted

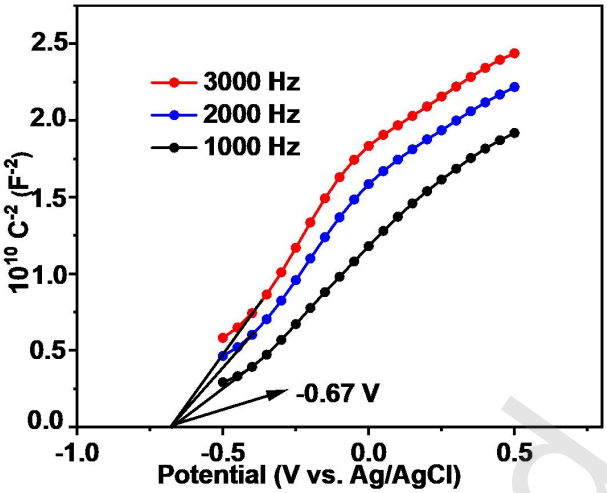

Figure S15. Mott-Schottky plots of NKU-332.

Just Accepted

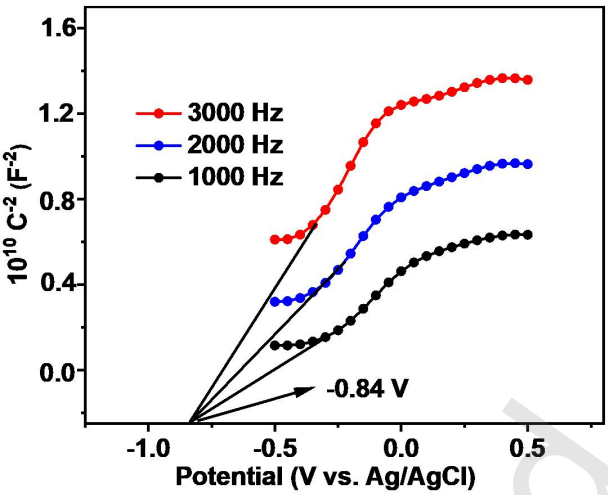

Figure S16. Mott-Schottky plots of NKU-333.

Just Accepted

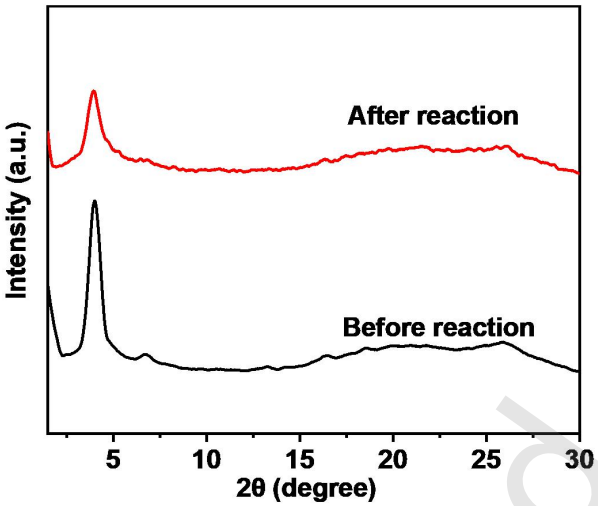

Figure S17. PXRD of NKU-331 before and after the photocatalytic reaction.

Just Accepted

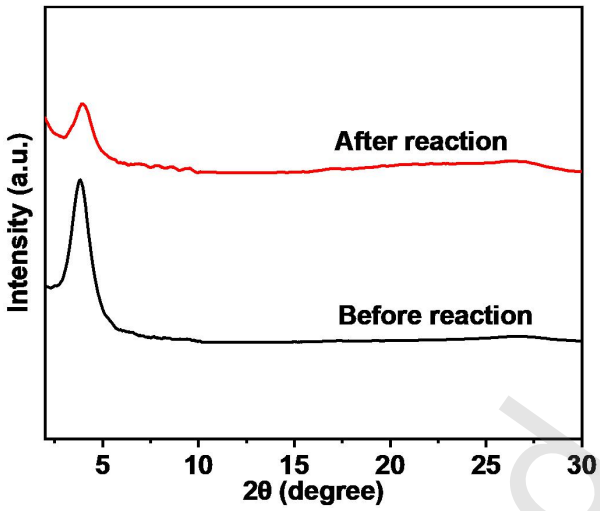

Figure S18. PXRD of NKU-332 before and after the photocatalytic reaction.

Just Accepted

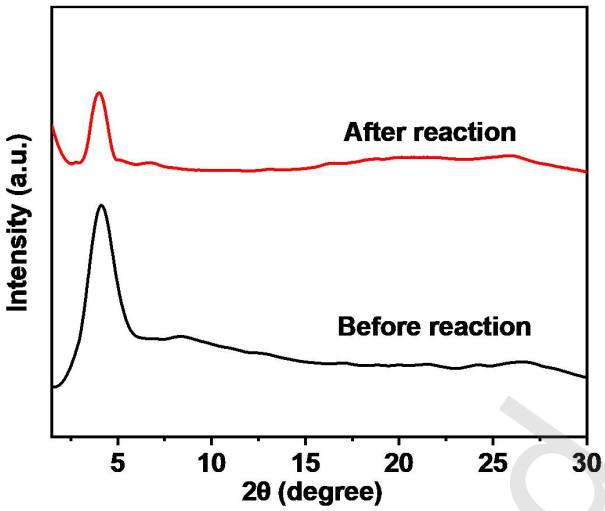

Figure S19. PXRD of NKU-333 before and after the photocatalytic reaction.

Just Accepted

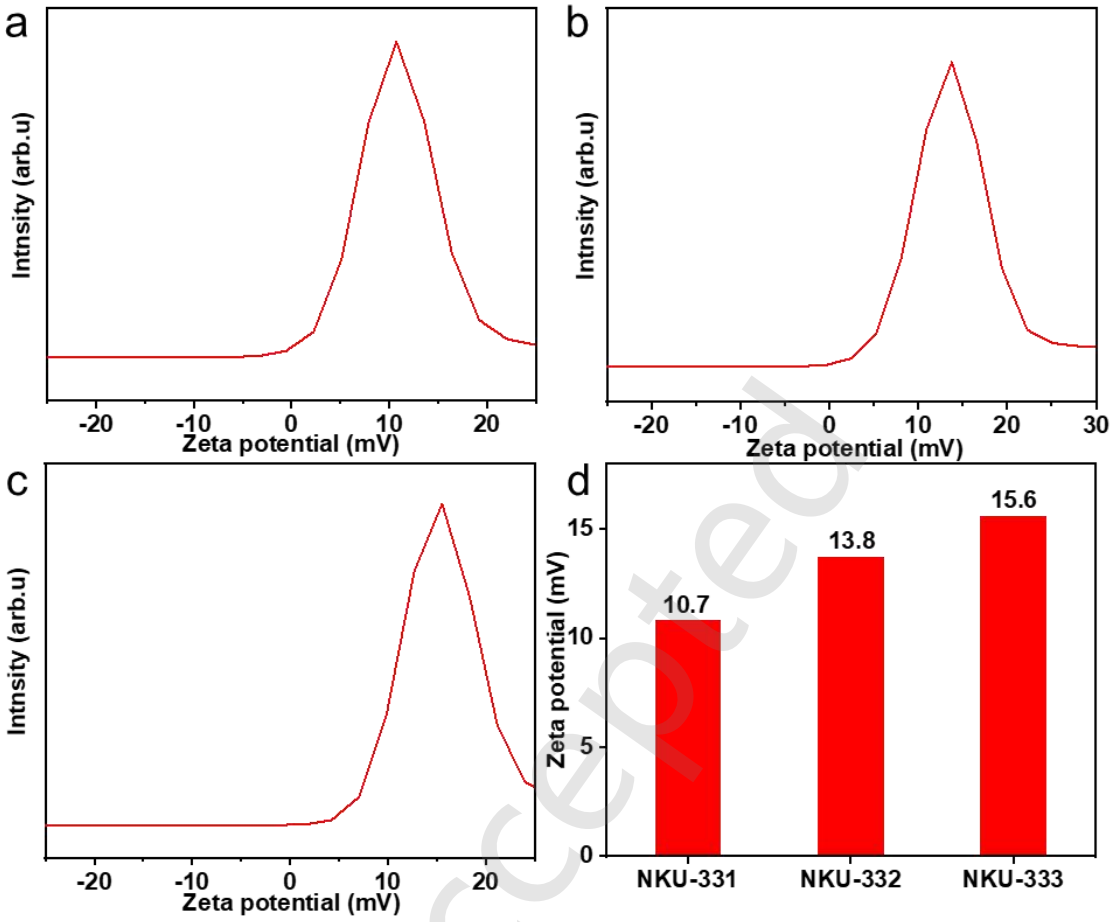

Figure S20. The zeta potential measurements of (a) NKU-331, (b) NKU-332 and (c) NKU-333. (d) The zeta potentials of NKU-331, NKU-332 and NKU-333.

Just Accepted

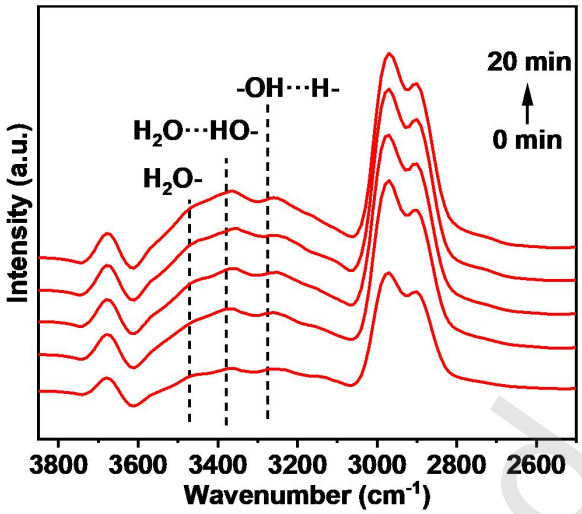

Figure S21. In situ DRIFTS spectra of NKU-331 gathering water vapor process.

Just Accepted

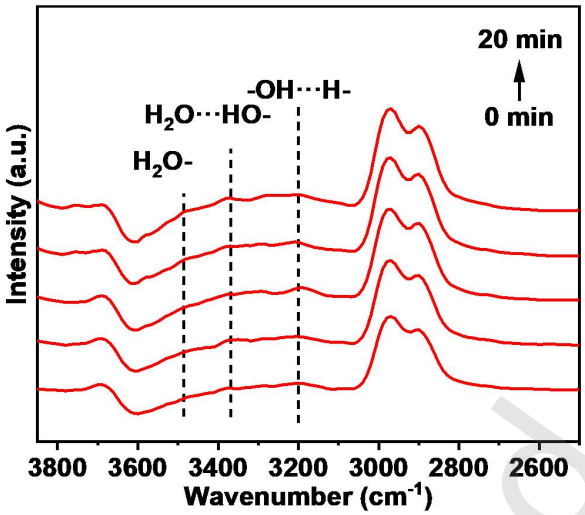

Figure S22. In situ DRIFTS spectra for NKU-332 gathering water vapor process.

Just Accepted

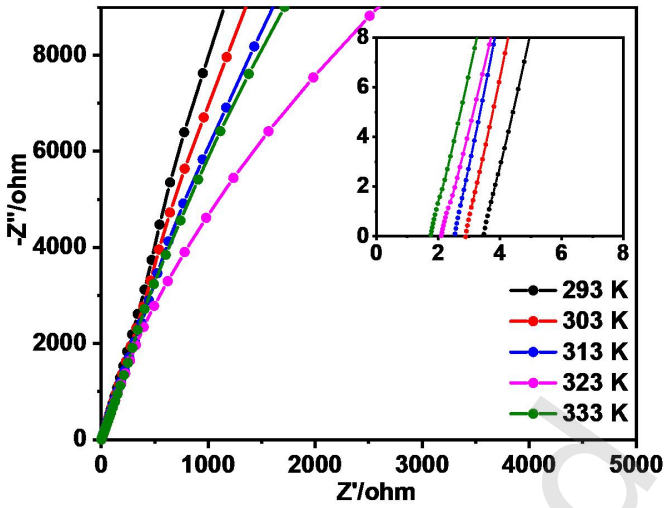

Figure S23. Temperature-dependent proton conductivity measurements for the NKU-331 film.

Just Accepted

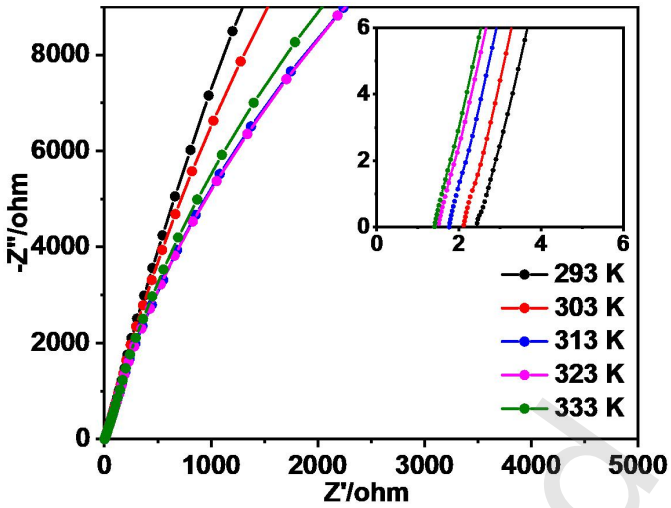

Figure S24. Temperature-dependent proton conductivity measurements for the NKU-332 film.

Just Accepted

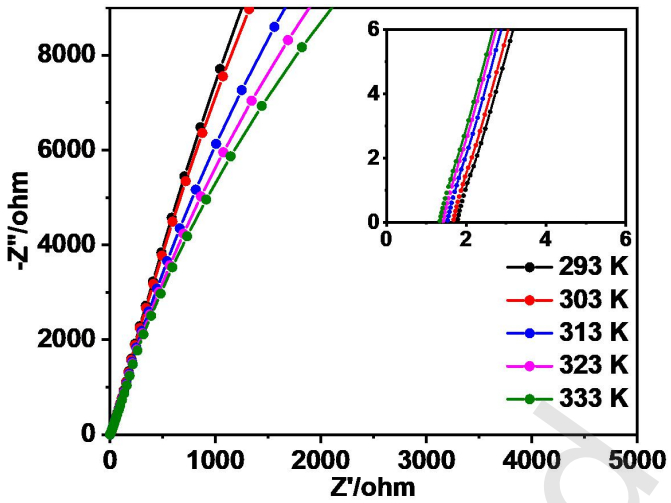

Figure S25. Temperature-dependent proton conductivity measurements for the NKU-333 film.

Just Accepted

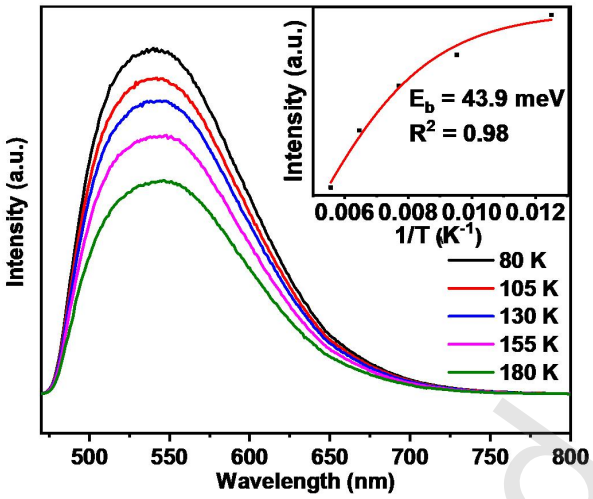

Figure S26. Temperature-dependent PL spectra from 80 to 180 K and fitted exciton binding energy of NKU-331.

Just Accepted

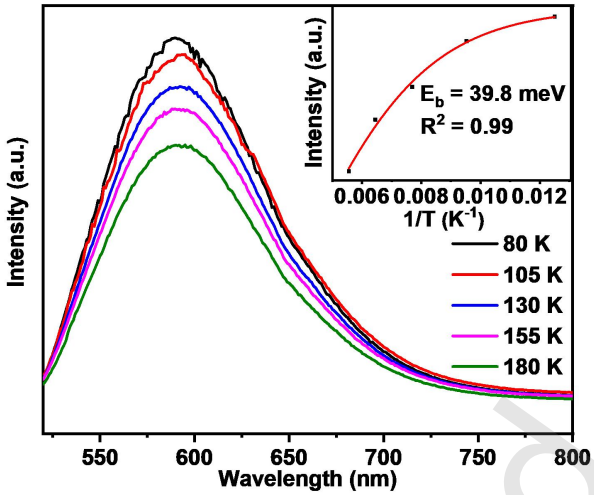

Figure S27. Temperature-dependent PL spectra from 80 to 180 K and fitted exciton binding energy of NKU-332.

Just Accepted

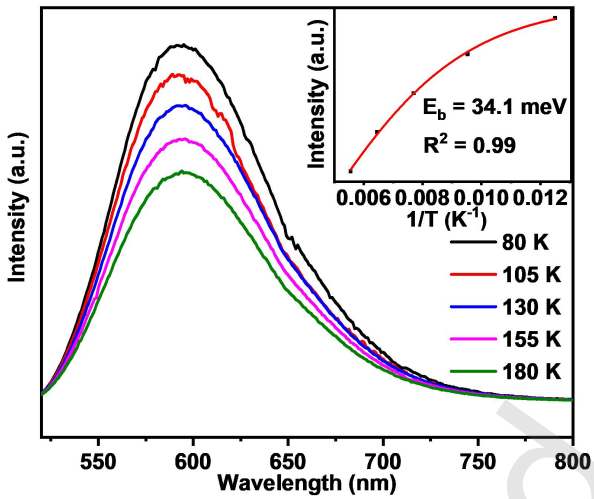

Figure S28. Temperature-dependent PL spectra from 80 to 180 K and fitted exciton binding energy of NKU-333.

Just Accepted

Table S1. Comparison of photocatalytic water splitting activities of COF-based photocatalysts.

Catalysts	Production (mg)	Bandgap (eV)	Experimental conditions	H_2 production ($\mu mol\ g^{-1}\ h^{-1}$)	AQE (%)	References
NKU-331	1150	2.30	λ > 420 nm; AA;	2300	0.22 (435 nm)	This work
NKU-332	1140	2.06	Pt (10 wt%); H_2O	9400	0.45 (450 nm)	
NKU-333	1160	2.02		31800	1.73 (450 nm)	
PtSA@S-TFPT	28	2.30	λ > 420 nm; TEOA; Pt (6.2 wt%); MeOH/H_2O (v/v = 1:3.5)	11401	4.65 (420 nm)	[6]
COF-Cu_3TG-Ru	< 45	1.76-2.34	λ > 420 nm; TEA; Ru; MeCN/H_2O	10470	0.42-0.62 (420 nm)	[7]
COF-C	24	2.31-2.42	λ > 420 nm; AA; Pt (8.0 wt%); H_2O: TEOA	31100	-	[8]
FS-COF	21	1.85	λ > 420 nm; AA; Pt (3.8 wt%); H_2O	10100	3.2 (420 nm)	[9]
BDDA-COFs	137	2.31	λ > 395 nm; TEOA; Pt (3.0 wt%); H_2O	324	1.8 (520 nm)	[10]
N_2-COF	50	2.6-2.7	TEOA; cobalt (8.0 wt%); H_2O	782	0.16 (400 nm)	[11]
COF-OMe-3	28	1.55-2.11	λ > 420 nm; AA; Pt (3.0 wt%); H_2O	23800	9.62 (450 nm)	[12]
TAPPy-DBTDP	20	2.18-2.29	λ > 420 nm; AA; Pt (9.0 wt%); H_2O	12700	5.0 (450 nm)	[13]
sp^2c-COF-ST	21	2.09-2.30	λ > 420 nm; TEOA; Pt (3.0 wt%); H_2O	2150	-	[14]
BTT-NDA	< 113	2.0-2.21	λ > 420 nm; AA; Pt (3.0 wt%); H_2O	5220	5.42 (420 nm)	[15]
TZ-COF-4	30	2.10-2.42	λ > 420 nm; AA; Pt (8.0 wt%); H_2O	4296	0.85 (420 nm)	[16]
PT-COF-	35	2.01-2.22	λ > 420 nm; AA; Pt (3.0	29290	2.51 (420 nm)	[17]

Just Accepted

OID			wt%); H_2O			
2D-COF-NO1	51	1.86-1.95	λ > 400 nm; AA; Pt (8.0 wt%); H_2O	1970	-	[18]
g-$C_{54}N_6$-COF	161	2.03-2.15	λ > 420 nm; TEOA; Pt (3.0 wt%); H_2O	2519	-	[19]
PyTz-COF	37	2.2-2.49	λ > 400 nm; AA; Pt (3.0 wt%); H_2O	2072	0.32 (450 nm)	[20]
BTH-3	26	-	λ > 420 nm; AA; Pt (8.0 wt%); H_2O	15100	0.79 (420 nm)	[21]
Py-ClTP-BT-COF	19	2.25-2.36	λ > 420 nm; AA; Pt (5.0 wt%); H_2O	8875	8.45 (420 nm)	[22]

Just Accepted

Table S2. Bi-exponential curve fitted parameters TRPL spectra for NKU-331–333.

Sample	A_1 (%)	τ_1 (ns)	A_2 (%)	τ_2 (ns)	τ_{ave} (ns)
NKU-331	87.69	0.21	12.31	0.83	0.28
NKU-332	90.00	0.29	10.00	1.32	0.39
NKU-333	96.14	0.34	3.86	3.53	0.46

The TRPL decay curves are fitted by bi-exponential fitting according to the following function:

$$I(t) = A_1 \cdot \exp(-t/\tau_1) + A_2 \cdot \exp(-t/\tau_2) \quad (1)$$

I is the normalized emission intensity, τ_1 and τ_2 are the lifetime values, A_1 and A_2 are corresponding constants indicating the amplitudes. A_1 (%) and A_2 (%) represent the percentage of the corresponding amplitudes [23, 24]. Then, on the basis of the above fitting data, the average lifetime (τ_{ave}) is calculated by following:

$$\tau_{ave} = A_1\,(\%) \cdot \tau_1 + A_2\,(\%) \cdot \tau_2 \quad (2)$$

Just Accepted

Table S3. Comparison of proton conductivity of different COFs reported in recent literature.

COFs	RH (%)	Additives for proton conductivity	Activation energy (*E*a)	Proton conductivity (S cm^{-1})	References
NKU-333	99	None	0.06 eV	2.97×10^{-3} (60 ℃)	This work
NKU-332	99	None	0.12 eV	2.72×10^{-3} (60 ℃)	This work
NKU-331	99	None	0.14 eV	2.57×10^{-3} (60 ℃)	This work
TFPPY-BT-COF-H_2PO_3	98	None	0.20 eV	1.12×10^{-3} (60 ℃)	[25]
CO_2–COF	95	None	0.28 eV	3.1×10^{-4} (85 ℃)	[26]
Br@CCOF	98	None	-	1.42×10^{-5} (100 ℃)	[27]
TG-DFP COF	99	None	0.04 eV	2.08×10^{-3} (100 ℃)	[28]
COF-LIFM7-Amide-N^+O^-	95	None	0.46 eV	1.90×10^{-3} (70 ℃)	[29]
COOH-COF-2	95	None	0.23 eV	2.60×10^{-3} (80 ℃)	[30]
Im-CH_3@COF	100	None	0.19 eV	2.40×10^{-3} (70 ℃)	[31]
H_3PO_4@PyTTA-BMTP	90	H_3PO_4	0.22 eV	7.1×10^{-2} (90 ℃)	[32]
PA-TpAzo	98	H_3PO_4	0.11 eV	9.9×10^{-4} (50 ℃)	[33]
H_3PO_4@PyHATP-1	98	H_3PO_4	0.18 eV	2.0×10^{-3} (80 ℃)	[34]

Just Accepted

References

[1] Zhang, S.; Lu, L.; Jiang, J.; Liu, N.; Zhao, B.; Xu, M.; Cheng, P.; Shi, W. Organizing photosensitive and photothermal single-sites uniformly in a trimetallic metal–organic framework for efficient photocatalytic hydrogen evolution. *Adv. Mater.* **2024**, *36*, 2403464.

[2] Liu, N.; Jiang, J.; Zhang, S.; Zhang, R.; Xu, M.; Chen, Z.; Cheng, P.; Shi, W. Arrangement of ordered D–A components in a metal-organic framework for cocatalyst-free photocatalytic hydrogen evolution with efficient proton conduction. *Angew. Chem. Int. Ed.* **2025**, *64*, e202501141.

[3] Jia, Z.; Ji, N.; Qi, J.; Wang, T.; Che, Y.; Zhao, Z.; Zhao, J.; Jiao, Z.; Wang, K.; Zhang, W.; Zhu, W.-H. Fused-heterocycle-linked covalent organic frameworks with enhanced chemical and photochemical stability for photocatalysis. *Angew. Chem. Int. Ed.* **2025**, *64*, e202511245.

[4] Frisch, M. J.; Trucks, G. W.; Schlegel, H. B.; Scuseria, G. E.; Robb, M. A.; Cheeseman, J. R.; Scalmani, G.; Barone, V.; Petersson, G. A.; Nakatsuji, H.; Li, X.; Caricato, M.; Marenich, A. V.; Bloino, J.; Janesko, B. G.; Gomperts, R.; Mennucci, B.; Hratchian, H. P.; Ortiz, J. V.; Izmaylov, A. F.; Sonnenberg, J. L.; Williams; Ding, F.; Lipparini, F.; Egidi, F.; Goings, J.; Peng, B.; Petrone, A.; Henderson, T.; Ranasinghe, D.; Zakrzewski, V. G.; Gao, J.; Rega, N.; Zheng, G.; Liang, W.; Hada, M.; Ehara, M.; Toyota, K.; Fukuda, R.; Hasegawa, J.; Ishida, M.; Nakajima, T.; Honda, Y.; Kitao, O.; Nakai, H.; Vreven, T.; Throssell, K.; Montgomery Jr., J. A.; Peralta, J. E.; Ogliaro, F.; Bearpark, M. J.; Heyd, J. J.; Brothers, E. N.; Kudin, K. N.; Staroverov, V. N.; Keith, T. A.; Kobayashi, R.; Normand, J.; Raghavachari, K.; Rendell, A. P.; Burant, J. C.; Iyengar, S. S.; Tomasi, J.; Cossi, M.; Millam, J. M.; Klene, M.; Adamo, C.; Cammi, R.; Ochterski, J. W.; Martin, R. L.; Morokuma, K.; Farkas, O.; Foresman, J. B.; Fox, D. J. Gaussian 16 Rev. C.01, Wallingford, CT, 2016.

[5] Zhang, Z.; Dong, X.; Yin, J.; Li, Z.; Li, X.; Zhang, D.; Pan, T.; Lei, Q.; Liu, X.; Xie, Y.; Shui, F.; Li, J.; Yi, M.; Yuan, J.; You, Z.; Zhang, L.; Chang, J.; Zhang, H.; Li, W.; Fang, Q.; Li, B.; Bu, X.; Han, Y. Chemically stable guanidinium covalent organic framework for the efficient capture of low-concentration iodine at high temperatures. *J. Am. Chem. Soc.* **2022**, *144*, 6821–6829.

[6] Chen, L.; Chen, G.; Gong, C.; Zhang, Y.; Xing, Z.; Li, J.; Xu, G.; Li, G.; Peng, Y. Low-valence platinum single atoms in sulfur-containing covalent organic frameworks for photocatalytic hydrogen evolution. *Nat. Commun.* **2024**, *15*, 10501.

[7] Li, J.; Zhou, J.; Wang, X.; Guo, C.; Li, R.; Zhuang, H.; Feng, W.; Hua, Y.; Lan, Y. In situ construction of single-atom electronic bridge on COF to enhance photocatalytic H_2 production. *Angew. Chem. Int. Ed.* **2024**, *63*, e202411721.

[8] Wang, W.; Tian, P.; Fu, Y.; Wan, X.; Lei, X.; Jia, C.; Liu, C.; Qi, Q.; Xu, S.; Zhao, X. Orthorhombic covalent organic frameworks with fmj topology as photocatalyst for hydrogen evolution. *Angew. Chem. Int. Ed.* **2025**, *64*, e202418086.

[9] Wang, X.; Chen, L.; Chong, S. Y. et al. Sulfone-containing covalent organic frameworks for photocatalytic hydrogen evolution from water. *Nat. Chem.*, **2018**, *10*, 1180-1189.

[10] Pachule, P.; Acharya, A.; Roeser, J.; Langenhahn, T.; Schwarzer, M.; Schomäcker, R.; Thomas, A.; Schmidt, J. Diacetylene functionalized covalent organic framework (COF) for photocatalytic hydrogen generation. *J. Am. Chem. Soc.* **2018**, *140*, 1423-1427.

[11] Banerjee, T.; Haase, F.; Savasci, G.; Gottschling, K.; Ochsenfeld, C.; Lotsch, B. V. Single-site photocatalytic H_2 evolution from covalent organic frameworks with molecular cobaloxime co-catalysts. *J. Am. Chem. Soc.* **2017**, *139*, 16228-16234.

[12] Luo, Z.; Zhu, S.; Xue, H.; Yang, W.; Zhang, F.; Xu, F.; Lin, W.; Wang, H.; Chen, X. Manipulating p-π resonance through methoxy group engineering in covalent organic frameworks for an efficient photocatalytic hydrogen evolution. *Angew. Chem. Int. Ed.* **2025**, *64*, e202420217.

[13] Liu, N.; Xie, S.; Huang, Y.; Lu, J.; Shi, H.; Xu, S.; Zhang, G.; Chen, X. Dual-acceptor engineering in pyrene-based covalent organic frameworks for boosting photocatalytic hydrogen evolution. *Adv. Energy Mater.* **2024**, *14*, 2402395.

[14] Fu, G.; Yang, D.; Xu, S.; Li, S.; Zhao, Y.; Yang, H.; Wu, D.; Petkov, P. S.; Lan, Z.; Wang, X.; Zhang, T. Construction of thiadiazole-bridged sp^2-carbon-conjugated covalent organic frameworks with diminished excitation binding energy toward superior photocatalysis. *J. Am. Chem. Soc.* **2024**, *146*, 1318-1325.

[15] Jeon, J.; Kim, Y.; Joo, S.; Noh, H.; Kwak, S.; Baek, J. Benzotrithiophene-based covalent organic framework photocatalysts with controlled conjugation of building blocks for charge stabilization. *Angew. Chem. Int. Ed.* **2023**, *62*, e202217416.

[16] Wang, K.; Jia, Z.; Bai, Y.; Wang, X.; Hodgkiss, S. E.; Chen, L.; Chong, S. Y.; Wang, X.; Yang, H.; Xu, Y.; Feng, F.; Ward, J. W.; Cooper, A. I. Synthesis of stable thiazole-linked covalent organic frameworks via a multicomponent reaction. *J. Am. Chem. Soc.* **2020**, *142*, 11131-11138.

[17] Huang, K.; Bai, J.; Shen, R.; Li, X.; Qin, C.; Zhang, P.; Li, X. Boosting photocatalytic hydrogen evolution through local charge polarization in chemically bonded single-molecule junctions between ketone molecules and covalent organic frameworks. *Adv. Funct. Mater.* **2023**, *33*, 2307300.

[18] Li, S.; Ma, R.; Xu, S.; Zheng, T.; Fu, G.; Wu, Y.; Liao, Z.; Kuang, Y.; Hou, Y.; Wang, D.; Petkov, P. S.; Simeonova, K.; Feng, X.; Wu, L.; Li, X.; Zhang, T. Direct construction of isomeric benzobisoxazole-vinylene-linked covalent organic frameworks with distinct photocatalytic properties. *J. Am. Chem. Soc.* **2022**, *144*, 13953-13960.

Just Accepted

[19] Xu, J.; Yang, C.; Bi, S.; Wang, W.; He, Y.; Wu, D.; Liang, Q.; Wang, X.; Zhang, F. Vinylene-linked covalent organic frameworks (COFs) with symmetry-tuned polarity and photocatalytic activity. *Angew. Chem. Int. Ed.* **2020**, *59*, 23845-23853.

[20] Li, W.; Huang, X.; Zeng, T.; Liu, Y. A.; Hu, W.; Yang, H.; Zhang, Y.; Wen, K. Thiazolo[5,4-d] thiazole-based donor–acceptor covalent organic framework for sunlight-driven hydrogen evolution. *Angew. Chem. Int. Ed.* **2021**, *60*, 1869-1874.

[21] Wang, Y.; Hao, W.; Liu, H.; Chen, R.; Pan, Q.; Li, Z.; Zhao, Y. Facile construction of fully sp^2-carbon conjugated two-dimensional covalent organic frameworks containing benzobisthiazole units. *Nat. Commun.* **2022**, *13*, 100.

[22] Chen, W.; Wang, L.; Mo, D.; He, F.; Wen, Z.; Wu, X.; Xu, H.; Chen, L. Modulating benzothiadiazole-based covalent organic frameworks via halogenation for enhanced photocatalytic water splitting. *Angew. Chem. Int. Ed.* **2020**, *59*, 16902-16909.

[23] Zhang, L.; Jin, Z.; Tsubaki, N. Zeolitic imidazolate framework-67-derived P-doped hollow porous Co_3O_4 as a photocatalyst for hydrogen production from water. *ACS Appl. Mater. Interfaces* **2021**, *13*, 50996-51007.

[24] Zhao, Z.; Wu, J.; Zheng, Y.; Li, N.; Li, X.; Tao, X. Ni_3C-decorated $MAPbI_3$ as visible-light photocatalyst for H_2 evolution from HI splitting. *ACS Catal.* **2019**, 9, 8144-8152.

[25] Lu, Z.; Yang, C.; He, L.; Hong, J.; Huang, C.; Wu, T.; Wang, X.; Wu, Z.; Liu, X.; Miao, Z.; Zeng, B.; Xu, Y.; Yuan, C.; Dai, L. Asymmetric Hydrophosphonylation of Imines to Construct Highly Stable Covalent Organic Frameworks with Efficient Intrinsic Proton Conductivity. *J. Am. Chem. Soc.* **2022**, *144*, 9624–9633.

[26] Zhang, S.; Lombardo, L.; Tsujimoto, M.; Fan, Z.; Berdichevsky, E. K.; Wei, Y.-S.; Kageyama, K.; Nishiyama, Y.; Horike, S. Synthesizing Interpenetrated Triazine-based Covalent Organic Frameworks from CO_2. *Angew. Chem. Int. Ed.* **2023**, *62*, e202312095.

[27] Liu, X.-F.; Huang, S.-Z.; Lian, Y.-X.; Dong, X.-Y.; Zang, S.-Q. Electrostatic attraction induces cationic covalent-organic framework to pack inorganic acid ions for promoting proton conduction. *Chem. Commun.* **2022**, *58*, 6084–6087.

[28] Das, G.; Shinde, D. B.; Melepurakkal, A.; Shelke, M. V.; Garai, B.; Bazin, P.; Ait Blal, A.; Benyettou, F.; Prakasam, T.; Abdul Halim, R.; Abou Ibrahim, F.; Sharma, S. K.; Varghese, S.; Weston, J.; Jagannathan, R.; Addicoat, M. A.; Gándara, F.; Olson, M. A.; El-Roz, M.; Trabolsi, A. Synergistic humidity-responsive mechanical motion and proton conductivity in a cationic covalent organic framework. *Chem* **2024**, *10*, 2500–2517.

[29] Wang, H.; Jiao, W.-N.; Zhu, W.-D.; Huang, S.; Lin, X.-C.; Chen, T.; Fan, Y.; Chen, F.; Xu, H.-S.; Pan, M.; Su, C.-Y. Stepwise Post-Modification of Pyridine-Imine COFs for Enhanced Hydrolytic Stability and Proton Conductivity. *Angew. Chem. Int. Ed.* **2025**, *64*, e202511559.

[30] Li, J.; Wang, J.; Shui, F.; Yi, M.; Zhang, Z.; Liu, X.; Zhang, L.; You, Z.; Yang, R.; Yang, S.; Li, B.; Bu, X.-H. Superhigh intrinsic proton conductivity in densely carboxylic covalent organic framework. *Chin. Chem. Lett.* **2023**, *34*, 107917.

[31] Zhang, K.; Wu, L.; Lan, K.; Zhang, Y.; Zhang, W.; Li, H.; Huang, G.; Wu, D.; Chen, L.; Li, M. N-3 of 1-methylimidazole: Enhancing proton conduction in COF under humidity conditions. *Chin. Chem. Lett.* **2026**, *37*, 111043.

[32] Liu, S.; Liu, M.; Li, X.; Xu, Q.; Sun, Y.; Zeng, G. Construction of dense H-bond acceptors in the channels of covalent organic frameworks for proton conduction. *J. Mater. Chem. A.* **2023**, *11*, 13965–13970.

[33] Chandra, S.; Kundu, T.; Kandambeth, S.; BabaRao, R.; Marathe, Y.; Kunjir, S. M.; Banerjee, R. Phosphoric Acid Loaded Azo (-N=N-) Based Covalent Organic Framework for Proton Conduction. *J. Am. Chem. Soc.* **2014**, *136*, 6570–6573.

[34] Luan, T.-X.; Wang, Q.; Zhang, P.; Li, W.; Kong, S.; Feng, Y.; Yuan, S.; Li, P.-Z. Remarkably enhancing proton conductivity by intrinsic surface sulfonation of a pyrazine-linked covalent organic framework. *Sci. China Mater.* **2024**, *67*, 125–133.

Just Accepted